Structure of the distal lung studied with inhaled nanoparticles

Petersson Sjögren, Madeleine

2023

Document Version:
Other version

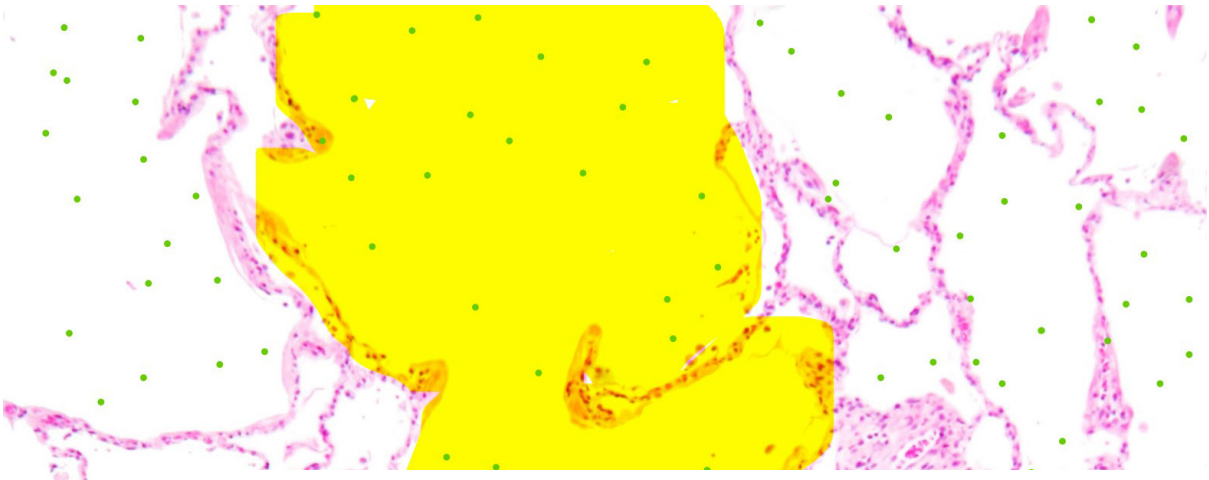

Structure of the distal lung studied with inhaled nanoparticles

MADELEINE PETERSSON SJÖGREN
DEPARTMENT OF DESIGN SCIENCES | FACULTY OF ENGINEERING | LUND UNIVERSITY

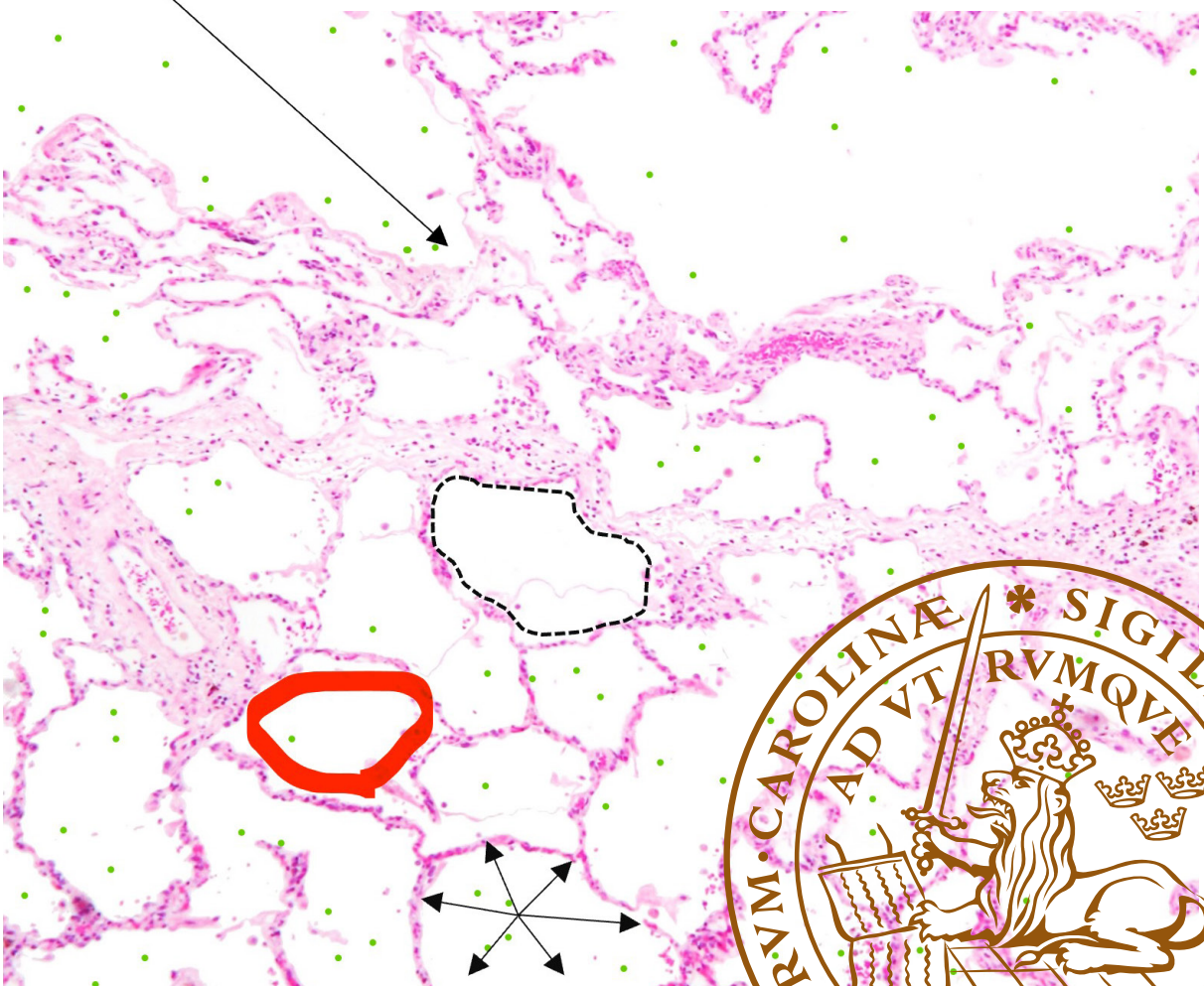

Structure of the distal lung studied with inhaled nanoparticles

Structure of the distal lung studied with inhaled nanoparticles

Madeleine Petersson Sjögren

LUND
UNIVERSITY

Doctoral dissertation by due permission of the Faculty of Engineering, Lund University. To be defended in Stora Hörsalen, IKDC on Friday, March 17, 2023 at 09:15.

Faculty opponent

Professor Torben Sigsgaard, Department of Public Health, Aarhus University

Organization	Document name
LUND UNIVERSITY Department of Design Sciences Box 118 SE–221 00 LUND Sweden	**DOCTORAL DISSERTATION** Date of disputation 2023-03-17 Sponsoring organization
Author(s) Madeleine Petersson Sjögren	

Title

Structure of the distal lung studied with inhaled nanoparticles

Abstract

Techniques able to detect impairments in the distal human lung are lacking. Since inhaled nanoparticles are predominantly deposited in the acini, their deposition can be used to derive structural properties of the region. In theory, structural enlargements in the distal lung imply that less inhaled nanoparticles deposit there. This rationale is the basis of the airspace dimension assessment (AiDA) method. The research presented in this thesis aimed to evaluate and characterize this new method for the measurement of distal lung structure. The objective was to do so by comparing the AiDA method with other lung structure and lung function measuring techniques as well as with background variables.

AiDA measurements were carried out with nearly 800 individuals in four different studies. From these, distal airspace radii (r_{AiDA}) were calculated, along with a second index: zero seconds recovery R_0.The AiDA method was benchmarked against magnetic resonance imaging (MRI) with hyperpolarized gas, with 23 healthy individuals and compared to computed tomography (CT) variables and standard pulmonary function tests (PFTs) in a population-based cohort with 695 subjects. The method was also evaluated as a tool to detect lung changes in an occupational group exposed to high loads of air pollution (with 28 welders and 17 controls), and AiDA indices were evaluated as parameters that can explain observed discrepancies between modeled and measured respiratory tract particle deposition in a group of 17 healthy participants.

The measured r_{AiDA} were correlated with lung microstructure measurements obtained with MRI with hyperpolarized gas and r_{AiDA} were on average larger in subjects with emphysema detected with CT, in comparison with healthy participants. The AiDA indices explained variance that no other PFTs captured, but there was no average difference between the occupational group and controls measurable with the AiDA method. The r_{AiDA} were correlated with the difference between measured and modeled respiratory tract particle deposition. Moreover, r_{AiDA} increased with age, but the inter-subject variability was large in all age groups.

The results demonstrated that the AiDA method has potential to characterize distal lung structure and may serve as a new, non-invasive tool for clinical examination of human lungs. However, the R_0 index needs to be further evaluated. In the future, controlled clinical trials are necessary to evaluate the method's sensitivity to different lung conditions.

Key words

nanoaerosols, particle-lung interactions, emphysema, respiratory diagnostics

Classification system and/or index terms (if any)

Supplementary bibliographical information	Language
	English
ISSN and key title	ISBN
	978-91-8039-539-7 (print) 978-91-8039-538-0 (pdf)
Recipient's notes	Number of pages: 156 / Price
	Security classification

Structure of the distal lung studied with inhaled nanoparticles

Madeleine Petersson Sjögren

LUND
UNIVERSITY

Cover illustration: Figure adapted from Michael Bonert. Re-used with rights.

Faculty of Engineering, Department of Design Sciences

ISBN: 978-91-8039-539-7 (print)
ISBN: 978-91-8039-538-0 (pdf)

Printed in Sweden by Media-Tryck, Lund University, Lund 2023

Contents

List of publications

This thesis is based on the following papers, referred to by their Roman numerals:

I **Airspace Dimension Assessment (AiDA) by inhaled nanoparticles: benchmarking with hyperpolarised ^{129}Xe diffusion-weighted lung MRI**
M. Petersson Sjögren†, H. F. Chan†, G. J. Collier, G. Norquay, L. E. Olsson, P. Wollmer, J. Löndahl, and J. M. Wild
Scientific Reports, 2021

II **Airspace dimension assessment with nanoparticles as a proposed biomarker for emphysema**
H. L. Aaltonen, **M. Petersson Sjögren**, J. Jakobsson, S. Diaz, V. Ideböhn, G. Engström, J. Löndahl, and P. Wollmer
Thorax, 2021

III **Airspace Dimension Assessment with Nanoparticles (AiDA) in Comparison to Established Pulmonary Function Tests**
M. Petersson Sjögren, H. L. Aaltonen, H. Nicklasson, J. Rissler, G. Engström, P. Wollmer, and J. Löndahl.
International Journal of Nanomedicine, 2022

IV **Sensitive methods for assessment of lung health in welders and controls**
M. Petersson Sjögren, M. Kåredal, K. Broberg, E. Assarsson, S. Thuresson, K. Dierschke, M. Hedmer, J. Rissler, P. Wollmer, and J. Löndahl
Under revision with Respiratory Medicine

V **An experimental study on lung deposition of inhaled 2 µm particles – in relation to lung characteristics and deposition models**
J. Rissler, **M. Petersson Sjögren**, J. Linell, P. Wollmer, and J. Löndahl
Manuscript

Papers I-III are reproduced with permission from their respective publishers.

† Shared first authorship

Author contributions

Paper I:

I had a major role in planning and implementing the study. I wrote the ethical application and recruited participants. I analyzed the AiDA data, did the statistical analysis and wrote the paper with the other first author.

Paper II:

I analyzed the AiDA data and was responsible for development of criteria for data quality control. I co-authored the article and took parts in discussions leading up to it.

Paper III:

I analyzed the AiDA data, compiled all data, planned, and performed the statistical analysis and wrote all parts of the paper.

Paper IV:

I took part in planning the study, analyzed the AiDA data, compiled all data and did the statistical analysis. I planned and wrote all parts of the paper.

Paper V:

I took part in planning the study and wrote the ethical application for it. I analyzed the AiDA data, conducted the statistical analysis, planned and wrote several parts of the paper.

Papers not included in the thesis

Measurement report: Atmospheric fluorescent bioaerosol concentrations measured during 18 months in a coniferous forest in the south of Sweden
M. Petersson Sjögren, M., T. Santl-Temkiv, T. Bjerring Kristensen, J. Löndahl
Under revision with Atmospheric Chemistry and Physics

Airspace Dimension Assessment (AiDA) for early detection of lung function impairment in the peripheral airways of firefighters
M. Kisiel, G. Cai, **M. Petersson Sjögren**, J. Löndahl, J. Jakobsson, P. Wollmer, A. Malinovschi, M. Svartengren
Accepted for publication with European Respiratory Journal Open Research

Abbreviations and symbols

α	Alpha heterogeneity index
ADC	Apparent diffusion coefficient
AiDA	Airspace dimension assessment
COPD	Chronic obstructive pulmonary disease
CPC	Condensation particle counter
CT	Computed tomography
D	Diffusion coefficient
DDC	Distributed diffusivity coefficient
DF	Deposited fraction
D_{LCO}	Diffusing capacity of CO
DMA	Differential mobility analyzer
DW	Diffusion-weighted
ERV	Expiratory reserve volume
FEV_1	Forced expiratory volume in 1 s
FRC	Forced residual capacity
FVC	Functional residual capacity
ICRP	International Commission on Radiological Protection
LAV	Low attenuation volume
Lm	Mean linear intercept length
Lm_D	Mean diffusion length scale
MPPD	Multiple path particle dosimetry
MRI	Magnetic resonance imaging
NCRP	National Council on Radiation Protection and Measurements
PCA	Principal component analysis
PD_{15}	15th percentile cut-off
PFT	Pulmonary function test
PS	Polystyrene
R_0	Zero seconds recovery
R_{rs}	Respiratory resistance
r_{AiDA}	AiDA-derived airspace radius
RV	Residual volume
SCAPIS	Swedish CArdioPulmonary bioImage study
$t_{1/2}$	Particle half-life time in the lungs
TLC	Total lung capacity
TV/V_{t}	Tidal volume
t_{res}	Particle lung residence time
$t_{\mathrm{instrument}}$	Particle residence time in the instrument
VC	Vital capacity
V_{tot}	Total inhaled volume
X_{rs}	Respiratory reactance

Acknowledgements

Many people have supported me and taught me things during these last couple of years. Firstly, I want to thank my supervisor Jakob Löndahl for his invaluable guidance and support: thank you for your encouragement and for sharing your enthusiasm for research. Thank you for being open for discussions about everything, including worries, ideas, ethics, research mentality, and everything else surrounding my life as a PhD student. Thank you Per Wollmer for taking the time to share your inspiring expertise and outstanding joy regarding physiology, particle-lung interactions and research! Thank you Jenny Rissler for your advice, your enthusiasm, for sharing your experiences openly and for actively and critically listening to me.

I want to thank my fellow PhD students, and other non (or-almost)-senior research colleagues, for these last couple of years: Thank you, Sara Thuresson, Julia Linell, Camilla Abrahamsson, Lovisa Nilsson, Malin Alsved, Vilhelm Malmborg, Hugo Öhrneman, Jonas Enarsson, Jonas Jakobsson, Calle Pregel, and Johannes Rex. Thank you all other colleagues, collaborators and friends! Thank you, Joakim Pagels, Aneta Wierzbicka, Christina Isaxon, Axel Eriksson, Patrik Nilsson, Erik Swietlicki, Adam Kristensson, Erik Ahlberg, Pontus Roldin, Thomas Bjerring-Kristensen, and Birgitta Svenningsson. Thank you Lars Erik Olsson for taking the time to discuss the MRI measurements and for reading parts of this thesis. Thank you, Haris for making the AiDA measurements possible. Thank you Pernilla Borgström for listening to my babbling over these last couple of years.

Thank you to my family for overwhelming love and support. Thank you to my father Stefan for sharing your joy and enthusiasm for research ever since I was I child. I never would have done a PhD if it was not for you. Thank you mother Cicki for inspiring me to take chances and to learn languages, and for always viewing the world with such a positive attitude. Thank you to my sister Ulrika for understanding everything. Thank you Nils Nilsson for unfailing optimism and for growing the family. Thank you Vera and Hugo, for bringing joy and happiness only children have the ability to spark. Thank you to my extended family; thank you Camilla and Roland for always showing interest in my work and for being enthusiastic about it. Thank you, Claes and Suzanna, for all wonderful and fun dinners. Thank you, Alle and Tess, for all fun times and travels

Thank you Tova Troedsson for our long friendship, I don't know who I would have been without you. Thank you Sara Sundén, Tora Hagsund, Anna Lundman, and Julia Molander for all fun times and for always being there for me! Thank you, Sonia Bastigkeit Ericstam, Nils Ekman, Maria Mårtenson, Adam Johansson, Evelina Linnros, Anna Török, Sofia Broomé, Victor Sardwall, and Amanda Eriksson. You are all very very very dear and important to me!

Thank you Adam Lexar for everything.

Popular Summary

Chronic obstructive pulmonary disease (COPD) is a major cause of morbidity and mortality in adults and has important health economic consequences. Globally, COPD is presently the third most common cause of death, and the prevalence of the disease is increasing. The disease mainly involves varying degrees of two physiologically different conditions: 1) narrowing of airways and 2) destruction of the smallest structural units in the lungs, the alveoli, in the form of emphysema. Early stages of COPD are relatively asymptomatic and thus diagnosis of the disease is often made when there is already an appreciable decrease in lung function and symptomatic deterioration. One reason as to why COPD is underdiagnosed is that it is very difficult to detect the structural changes in the peripheral lungs associated with emphysema early.

The number of inhaled particles that deposit in the peripheral regions of the lungs depends on the structure of that lung. In a healthy lung, the alveoli are well-defined, small cavities that maximize the surface area available for gas exchange. Emphysema causes the alveolar walls to break down, creating large, hollow cavities with less surface area available for gas exchange. As a result, inhaled particles have fewer surfaces to adhere to in a lung with emphysema compared to in a healthy lung. By measuring the number of particles that deposit in the peripheral lung, conclusions can be drawn on the size of the cavities in the peripheral lungs. This rationale is used in the *airspace dimension assessment* (AiDA) method.

With the AiDA method, a low concentration of nanoparticles is inhaled, followed by a breath-hold, and then the number of exhaled particles are measured. From these measurements, a metric of the distal lung structure is calculated: airspace radius (r_{AiDA}). To evaluate the potential of such measurements, the AiDA method was in the research presented here compared to other techniques for measurement of lung structure and lung function. The results of the AiDA measurements were compared to those provided with magnetic resonance imaging (MRI) with hyperpolarized gas, with computed tomography (CT) and with conventional pulmonary function tests (PFTs). AiDA measurements were also evaluated in an occupational group susceptible to lung diseases and AiDA indices were explored as parameters that could be used to explain the differences observed between measured and modeled respiratory particle deposition.

The results presented here indicate that the AiDA measurements agreed with MRI measurements of distal lung microstructures. The measured radii r_{AiDA} were larger in subjects that had emphysema according to CT and it was shown that AiDA measurements hold information beyond that provided with conventional PFTs. However, no differences were identified between the occupational group and the controls using AiDA. Altogether, the research results showed that measurements of inhaled deposited nanoparticles with the AiDA method can potentially by used as a biomarker for emphysema.

Populärvetenskaplig sammanfattning

Konisk obstruktiv lungsjukdom (KOL) är en av vår tids stora folksjukdomar. Globalt är idag KOL den tredje största dödsorsaken och prevalensen av sjukdomen ökar. År 2019 dog mer än 3 miljoner människor på grund av KOL och i Sverige uppskattas mellan 400 000 och 700 000 personer lida av sjukdomen. KOL orsakar kroniska förändringar på lungvävnaden: ledande luftvägar blir förträngda och de minsta strukturerna i lungan (alveolerna) bryts ner. När alveolerna bryts ner förstörs den perifera lungans struktur, vilket bildar hålrum, så kallat lungemfysem. Lungemfysem är kroniskt, men om förändringarna i lungan kan upptäckas tidigt är chanserna större för att stoppa sjukdomsutvecklingen.

De strukturella förändringarna som lungemfysem innebär är svåra att identifiera i ett tidigt stadie av sjukdomsförloppet. Detta beror i stor utsträckning på att konventionella lungfunktionsmätningar är okänsliga för strukturella förändringar i den perifera lungan. Ofta kommer sjukdomssymptomen förknippade med lungemfysem smygande, vilket leder till att olika sjukdomstillstånd blandas ihop och feldiagnosticeras, samt att både diagnos och korrekt behandling försenas.

Kunskapen om att små inandade partiklar når perifer lunga skulle kunna användas för att mäta perifer lungas struktur. Genom att mäta hur många inandade partiklar som fastnar i lungorna kan man med kunskap om partiklarnas egenskaper och patientens uppmätta andningsmönster dra slutsatser om strukturen i perifer lunga.

I en frisk lunga är alveolerna små och väldefinierade, så att ytan hos varje alveol är tillgänglig för syreupptagning. Håligheterna i perifer lunga som bildas vid lungemfysem orsakar försämrad syreupptagning, men gör också att små inandade partiklar har färre ytor att fastna på. Följaktligen leder lungemfysem till att färre partiklar fastnar i den perifer lungan, och att en större andel partiklar följer med utandningsluften. Från mätningar av hur många partiklar som fastnar i den perifera lungan kan man därför beräkna hur stora håligheterna i den perifera lungan är, och alltså få ett mått på dess struktur. Denna princip ligger till grund för *airspace dimension assessment* (AiDA)-tekniken som testats och utvärderats i detta avhandlingsarbete.

AiDA-metoden bygger på att en låg koncentration luftburna nanopartiklar andas in, följt av en kort andhållning, och därefter noggrann mätning av hur många partiklar som följer med utandningsluften. Från mätningen av hur många nanopartiklar som fastnar i lungan beräknas ett storleksmått på den perifera lungans struktur, en radie: r_{AiDA}. För att förstå hur väl r_{AiDA} avspeglar den perifera lungans struktur har r_{AiDA} i det här arbetet jämförts med etablerade mätningar av lungans struktur och funktion.

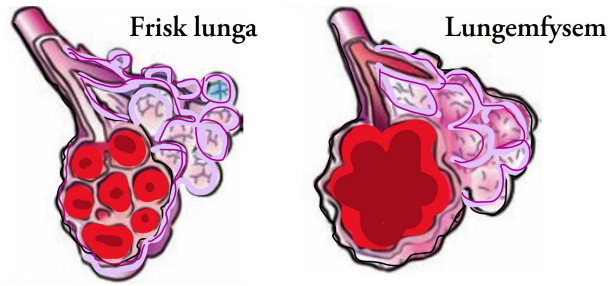

I en frisk lunga är alveolerna små och väldefinierade. I en lunga med emfysem har alveolernas struktur förstörts vilket bildar förstorade håligheter. De förstorade håligheterna ger försämrad syreupptagning och färre ytor för inandade partiklar att fastna på.

För detta ändamål genomfördes AiDA-experiment med närmare 800 individer i fyra olika studier. I den första studien jämfördes r_{AiDA} med andra mätningar av perifera lungans struktur: magnetresonanstomografi (MRI) med hyperpolariserad gas. I den andra studien jämfördes r_{AiDA} med lungröntgen och konventionella lungfunktionsmätningar. I den tredje studien utvärderades AiDA-metodens känslighet för förändringar i den perifera lungan hos en yrkesgrupp som exponeras för höga halter luftföroreningar: svetsare. I den fjärde studien utvärderades r_{AiDA} som parameter för att förstå skillnader mellan uppmätt och modellerad partikeldeponering i människors lungor.

Resultaten som här presenteras indikerade att r_{AiDA} kan användas för att mäta strukturen i den perifera lungan. Jämförelsen mellan AiDA och MRI visade att r_{AiDA} stämde överens med andra mått på den perifera lungans struktur. Bland individer som hade lungemfysem enligt lungröntgen var r_{AiDA} större jämfört med r_{AiDA} i friska individer. AiDA mätningarna visade ingen skillnad mellan svetsare och kontrollgruppen, vilket kan tolkas som att svetsarna över lag inte hade strukturella förändringar i den perifera lungan. Mätningarna indikerade också att r_{AiDA} var relaterade till skillnader mellan modellerade och uppmätta andelar partiklar som fastnar i lungorna, vilket visade att r_{AiDA} skulle kunna användas för att förbättra lungdeponeringsmodeller.

Eftersom lungemfysem är obotligt är det viktigt att upptäcka sjukdomen i ett tidigt stadium för att kunna påbörja behandling och försöka bryta sjukdomsutvecklingen. AiDA metoden som här utvärderats skulle i framtiden kunna användas för att upptäcka lungemfysem tidigare än vad som idag är möjligt inom sjukvården.

Structure of the distal lung studied with inhaled nanoparticles

1 Introduction

Inhaled aerosol particles are deposited in the respiratory tract to varying degrees. The three major factors determining where inhaled particles end up are: lung properties, including the lung structure, particle characteristics, and breathing patterns. Linkage between these factors can be used to derive lung properties from particle deposition measurements. The smallest airborne particles are nanoparticles, loosely defined as all particles with d_p <100 nm. A large fraction of all inhaled nanoparticles will follow the inspiratory flow and deposit in the distal lung.

The distal airspaces in the lungs are the structural units located distally to the terminal bronchioles. The surfaces of the alveoli in the distal airspaces make up the pulmonary blood-gas barrier, which serves as the site for oxygen and carbon dioxide exchange between the lungs and the pulmonary vasculature. The exquisite thinness of the blood-gas barrier, and the small diameters of the distal airspaces, make this region a site for pathological responses in the form of destruction and remodeling due to inhaled pollutants and noxious agents (Higham et al., 2019).

Detection of structural changes in the distal airspaces is crucial for clinical evaluation and longitudinal monitoring of a range of pulmonary diseases. The fact that inhaled nanoparticles reach the distal lung makes these particles potential agents for the measurement of distal airspace structures.

The aim of this thesis was to evaluate and characterize a new method for measurement of distal airspace structures. The method is called *airspace dimension assessment*, or in short: AiDA. The underlying idea of the method is to derive distal airspace radius from nanoparticle lung deposition measurements. An average distal airspace radius is derived by combining a model that describes the behavior of nanoparticles in distal airspaces with

measurement of how many particles that are deposited.

The underlying hypothesis in this work was that inhaled nanoparticles can be used to estimate distal airspace radius. To address this, nanoparticle deposition-derived indices were compared to other lung structure and function measurements. The two core questions that I set out to answer were: *How do the derived airspace radii compare with other measurements of lung structure and function?* and *Do nanoparticle lung deposition measurements contain information beyond that obtained with conventional pulmonary function tests?*

Objectives

The objective of this thesis was to evaluate the airspace dimension assessment (AiDA) method by comparing it with other techniques for measurements of lung structure and lung function. The objective can be separated into the following five main parts:

- Benchmark the AiDA method against another technique for in vivo measurement of distal lung structure: diffusion-weighted magnetic resonance imaging with hyperpolarized gas (**Paper I**).
- Evaluate AiDA as a biomarker for emphysema by comparing AiDA indices to chest computed tomography results and pulmonary function measurements (**Papers II and III**).
- Compare the AiDA derived indices to background variables (**all five papers**).
- Test the capability of detecting early pathological changes due to occupational exposure with AiDA (**Paper IV**).
- Explain differences between modeled and experimentally measured particle deposited fractions with the AiDA indices (**Paper V**).

2 Background

Particulate aerosols are liquid or solid particles that are ubiquitous in the atmosphere and air that humans breathe. The main route through which aerosol particles enter the human body is by inhalation. An adult breathes over 10 000 liters of air daily. Hence, a large number of particles passes through each and everyone's respiratory tract every day. Where the inhaled particles deposit depends on particle characteristics, breathing patterns and individual anatomical variations.

The use of inhaled nanoparticles to derive structural properties of the distal lung relies on information about the structure of the respiratory tract and the behaviour of the inhaled particles in that structure.

To evaluate how nanoparticle lung deposition measurements fit into the already existing scheme of pulmonary function tests and lung structure measurements, one needs to understand what information that is already attainable with such techniques. Therefore, this background section covers three parts: 1) an overview of the human respiratory tract with focus on the lower respiratory tract, 2) a review of particle lung interactions, and 3) a survey of measurement techniques that can be (and were in this work) used to derive information about lung structure and lung function.

2.1 Structure of the respiratory tract and breathing

The main function of the respiratory tract is to deliver oxygen from inhaled air to the bloodstream and remove carbon dioxide. In the deep lungs, air and blood are brought in close proximity so that oxygen molecules can diffuse across the interface between the lungs and the blood stream capillaries. The total surface area available for this gas exchange is about 100 m^2 in an adult. From the capillaries, oxygen is transferred to all parts of the body while CO_2 is removed with exhaled air.

The respiratory tract is divided into three structurally different regions: upper airways, conducting airways and the respiratory region. In the upper airways (the nose, the mouth, the paranasal sinuses, the pharynx, and the larynx) airflows are generally turbulent (Doorly et al., 2008; Wang, 2005). Here, inhaled air is conditioned to body temperature and almost completely saturated (99.5% relative humidity) with water vapor.

The conducting airways and respiratory region, which together form *the lower respiratory tract*, bifurcate over 24 airway generations, from trachea down to alveoli. In the restricted sense here used, lungs refer to everything from the bronchi down to the alveoli, hence excluding the upper airways and trachea.

Table 1: The lower respiratory tract: conducting airways and respiratory region, in terms of generations in Weibel's lung model (Weibel et al., 1963) showing the generation numbers of repeatedly bifurcating airways. The model is for an average adult at about 75% total lung capacity, at a constant airflow with a tidal volume of 1 L, and an inspiratory duration of 2 seconds.

Generation	Number of airways per generation	Airway diameter (cm)	Airway length (cm)	Total cross section (cm^2)	Number of alveoli per generation
0	1	1.80	12	2.54	
1	2	1.22	4.76	2.33	
2	4	0.83	1.90	2.13	
3	8	0.56	0.76	2.0	
4	16	0.45	1.27	2.48	
⋮	⋮	⋮	⋮	⋮	
14	16 384	0.074	0.23	69.4	
15	32 768	0.066	0.20	113.0	
16	65 536	0.060	0.165	180	
17	131 072	0.054	0.141	300	$6{\cdot}10^5$
18	262 144	0.050	0.117	543	$2{\cdot}10^6$
19	524 288	0.047	0.099	944	$6{\cdot}10^6$
20	1 048 576	0.045	0.083	1600	$21{\cdot}10^6$
21	2 097 152	0.043	0.070	3220	$42{\cdot}10^6$
22	4 194 304	0.041	0.059	5880	$84{\cdot}10^6$
23	8 388 608	0.041	0.050	11800	$143{\cdot}10^6$

Simplified lung models are used to describe the complexity of the lung structure. One of the most widely used models for the structure of the lower respiratory tract is Weibel's lung model (Weibel, 1991; Weibel et al., 1963), shown in Table 1 for an average adult at 75% of maximal inflation. The model illustrates the sequential relationship between consecutive airway generations. Generations 0 to ∼14 are conducting, generations 15-17 are transitional, while generation ∼18 and beyond comprise the respiratory region. The distal lung refers to all regions beyond generation ∼8. Distal airways are located after the 8th generation down to terminal bronchioles, and are defined by an internal <2 mm in adults (Burgel et al., 2009). Distal airspaces refer to all airspaces in the respiratory region, that is, distally to the terminal bronchioles

Conducting airways

Air reaches the respiratory region via the conducting airways, which do not take part in gas exchange. Their collected volume (together with non-aveolated respiratory bronchioles) makes up the anatomic dead space. The trachea and bronchi are relatively rigid with a large amount of cartilage in their walls and are lined by stratified ciliated epithelium and a layer of mucus, which covers nearly all surfaces of the conducting airways. With increasing

generations, the cross-sections of the airways increase (see Table 1), the epithelium height decreases, and the amount of cartilage decreases so that bronchioles are surrounded mostly by smooth muscles.

Airflow in the trachea and larger bronchi depends on ventilation and is generally turbulent and/or transitional. The rapid increase of the total cross-sectional area of the airways result in a sharp decrease in linear air velocity such that airflow in the distal lung is typically laminar (Wang, 2005).

The respiratory region

The respiratory region (also referred to as the lung parenchyma) comprises about 90% of the total lung volume. Each terminal bronchiole feeds into an acinus, which contains transitional bronchioles, respiratory bronchioles, alveolar ducts and alveoli. Alveoli start to appear in transitional bronchioles, respiratory bronchioles are mixtures of conducting airways and alveolar openings, while alveolar duct surfaces are entirely covered by alveolar sacs. A human adult lung contains about 400 million alveoli, the number of which is closely related to lung volume such that larger lungs contain considerably more alveoli. The mean size of a single alveolus is rather constant in the human lung, with an average diameter of about 200-250 µm (Ochs et al., 2004; Weibel, 2017). The diameter of the central channel in an acinus falls from 500 µm to the diameter of an average alveolus (Ochs et al., 2004; Papadakos and Lachmann, 2007; Weibel, 2017) . The alveolar walls are covered in a dense network of capillaries.

Alveoli are the main functional units of the lungs and lung inflation occurs due to expansion of the respiratory region. When a healthy human inhales, the volume increase is primarily due to alveolar recruitment and to a lesser extent, due to expansion of the alveoli and alveolar ducts (Hajari et al., 2012). For gas exchange to take place the alveoli must be ventilated, and perfusion of blood must take place in the alveolar wall capillaries. Due to the pressure gradient between the upper and lower lung, alveoli in the upper lung are well inflated but poorly ventilated, while in the lower lung the alveoli are more poorly inflated but well ventilated.

Laminar convective flow and diffusion govern gas movement in the acini (Hofemeier and Sznitman, 2015). While airflow is driven by pressure gradients, diffusion is driven by concentration gradients. The rate of diffusion depends on molecular weight, where light molecules such as hydrogen diffuse more rapidly than larger molecules. Model studies indicate that acinar airflow can be complex and chaotic due to the expansion of alveoli during breathing (Tsuda et al., 1995).

Lung function and lung structure change with advancing age. Most of the respiratory

tract is developed at birth but full multiplication of the alveoli is not complete until young adulthood (Schittny, 2017). From birth to adulthood, airway dimensions increase with a factor of about 3 while alveoli grow from about 50-100 µm to about 200-250 µm, in diameter. Many parts of the respiratory tract lose elastic retraction and increase in elasticity with advancing age. Moreover, distal airspaces grow in size naturally with age (Papadakos and Lachmann, 2007; Gillooly and Lamb, 1993) .

Emphysema changes the distal lung structure

Chronic obstructive pulmonary disease (COPD) is an umbrella term that refers to several lung conditions. Globally, there were more than 200 million cases of COPD in 2019, and in the same year more than 3 million people died from the disease (Adeloye et al., 2022). Moreover, the prevalence of COPD is expected to increase as the population ages (Burney et al., 2015), and the disease usually becomes apparent in middle to older age (Abramson et al., 2014). The main COPD conditions are chronic bronchial disease and emphysema, and COPD patients commonly have varying degrees of both conditions. While chronic bronchial disease is a condition of the conducting airways, emphysema affect the acini.

Emphysema is characterized by permanent destruction of alveoli walls, leading to loss of functional surface, loss of alveoli and enlargement of the distal airspaces (Thurlbeck, 1995). The condition is caused, and enhanced, by persistent inhalation of toxic particles derived from tobacco smoke and/or high concentrations of urban environmental air pollution or occupational exposures (Vogelmeier et al., 2017). Figure 1 shows a microscopic image of distal airspaces in an emphysematous lung where increased airspace size is visible on the left, while more preserved airspaces are visible to the right. In addition to decreasing the surface area available for gas exchange, the structural alterations due to emphysema cause disparity in the filling and emptying rates between different compartments of the lungs and hence heterogeneous ventilation. Despite being a leading cause of disability, emphysema often goes undiagnosed for many years and irreversibly destroys alveoli, cause hyperinflation and reduces lung elasticity (Minai et al., 2008) .

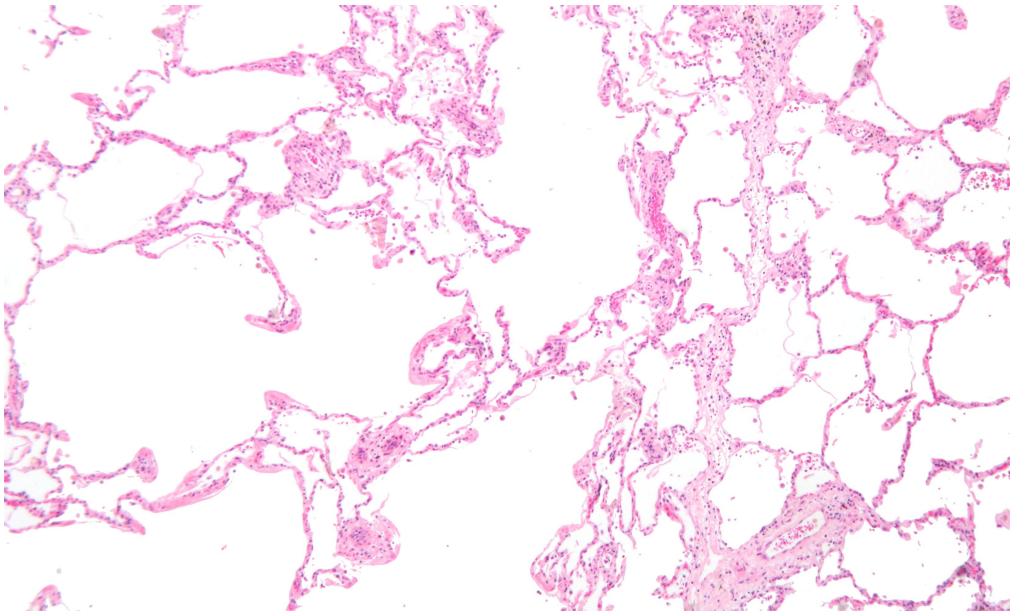

Figure 1: Low magnification micrograph of emphysematous human lung showing differences in airspace size for emphysematous changes (left) and relatively large preservation of alveoli (right). Image copyright Michael Bonert. Re-used with rights.

2.2 Particle-lung interactions

Inhaled particles travel with the airflow in the respiratory tract and deposit by different mechanisms and rates, throughout the system. Particle dispersion and deposition in the respiratory tract is determined by biological factors, such as lung structure and breathing patterns, and physical factors, such as particle properties (e.g., size, shape and ability to absorb water) and deposition mechanisms. In consequence, particles are dispersed, deposited and cleared at different rates and due to different mechanisms throughout the respiratory tract.

Ambient airborne particles are commonly between a few nm up to 100 µm in diameter (d_p). Inhaled particles that reach the lungs are typically below 10 µm (PM_{10}) in diameter. These include small particles (d_p <5 µm), fine particles (d_p <2.5 µm; $PM_{2.5}$), and ultrafine particles (d_p <100 nm, also referred to as nanoparticles).

Particle dispersion with airflow in the respiratory tract

The dispersion of aerosol particles depends on particle interactions with the surrounding gas. The motion of a particle moving in a fluid continuum is governed by the drag force, the gravitational force, and the force due to interactions with the surrounding gas molecules,

causing Brownian motion.

For particles with d_p >0.5 µm, the motion is governed by the ratio between drag forces and gravitational settling and the random motion due to Brownian motion is negligible for such particles. In conducting airways, where air velocity is high, the inertial force is more dominant than gravity, while gravity becomes increasingly important in smaller airways and in the acini. Gravitational settling depends on particle size, density, and residence time in a given geometry. If one neglects buoyancy, the settling velocity (V_S) for such a particle is given by:

$$V_S = \frac{d_p^2 g C_c \rho_p}{18\mu}, \tag{1}$$

where ρ_p is particle density, C_c is Cunningham's slip correction factor and μ is the viscosity of air.

Particles with d_p around 0.5 µm are too large for significant Brownian motion, and too small for significant inertial or gravitational crossing of streamlines. Consequently, they will closely follow the local gas velocity field so that over reversible breathing cycles there is approximately no net transport of these particles: they are inhaled and later exhaled to a large extent.

For particles with dp <0.5 µm, gravity is insignificant and the relaxation times are on the order of pico- to microseconds, such that the acceleration of the particles can be ignored. This makes the force due to Brownian motion, dampened only by viscous drag, the dominant force acting on small particles throughout the respiratory tract. Diffusion is governed by the diffusion coefficient D given by:

$$D = \frac{k_B T_{\mathrm{abs}} C_c}{3\pi\mu d_{\mathrm{p}}}, \tag{2}$$

where k_B is Boltzmann's constant and T_{abs} the absolute temperature. The diffusion coefficient is significantly smaller for aerosol particles than for typical respiratory gases. For example, the diffusivity of aerosol particles with d_p between 10-100 nm, are on the order of 10^{-4} to 10^{-6} $\mathrm{cm^2 s^{-1}}$, which is 2-4 orders of magnitude smaller than the diffusivity of O_2 and CO_2.

Brownian motion is driven by particle concentration gradients. The average distance that a group of particles travel in a time t due to Brownian motion in one dimension is given by the root mean square (rms) displacement:

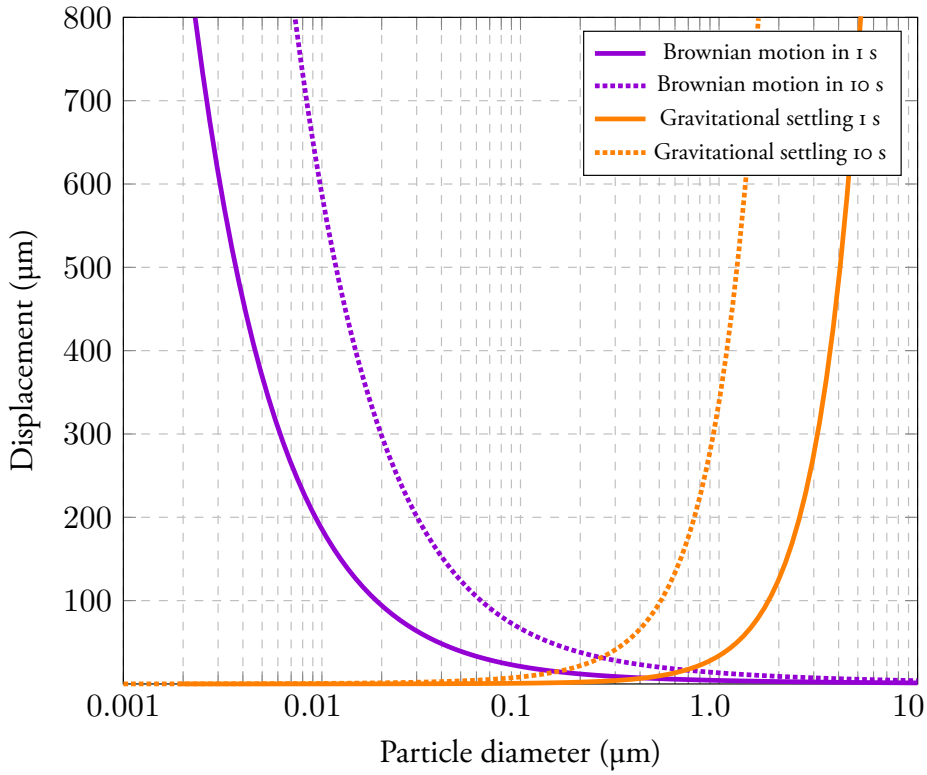

Figure 2: Displacement due to Brownian motion and gravitational settling for particles with diameters 10 nm to 10 µm in 1 and 10 seconds.

$$x_{\text{rms}} = \sqrt{2Dt} \tag{3}$$

Figure 2 shows the relative importance of gravitational settling and Brownian motion for particles in the size interval 10 nm to 10 µm, for 1 second and 10 seconds. The figure is based on Equations 1 and 3 at atmospheric pressure and body temperature, and shows the displacement in one dimension. While Brownian diffusion is the dominant mode of motion for particles $d_p \leq 1$ µm, settling due to gravity increases exponentially for particles $d_p > 1$ µm.

Particle deposition in the respiratory tract

When particles encounter airway walls they deposit. The deposition of inhaled particles is mainly a result of impaction, gravitational settling, and diffusion. Figure 3 shows the estimated total and regional deposited fraction of inhaled particles with diameters between 10 nm and 100 µm. The curves were generated with equations from Hinds (1999), for

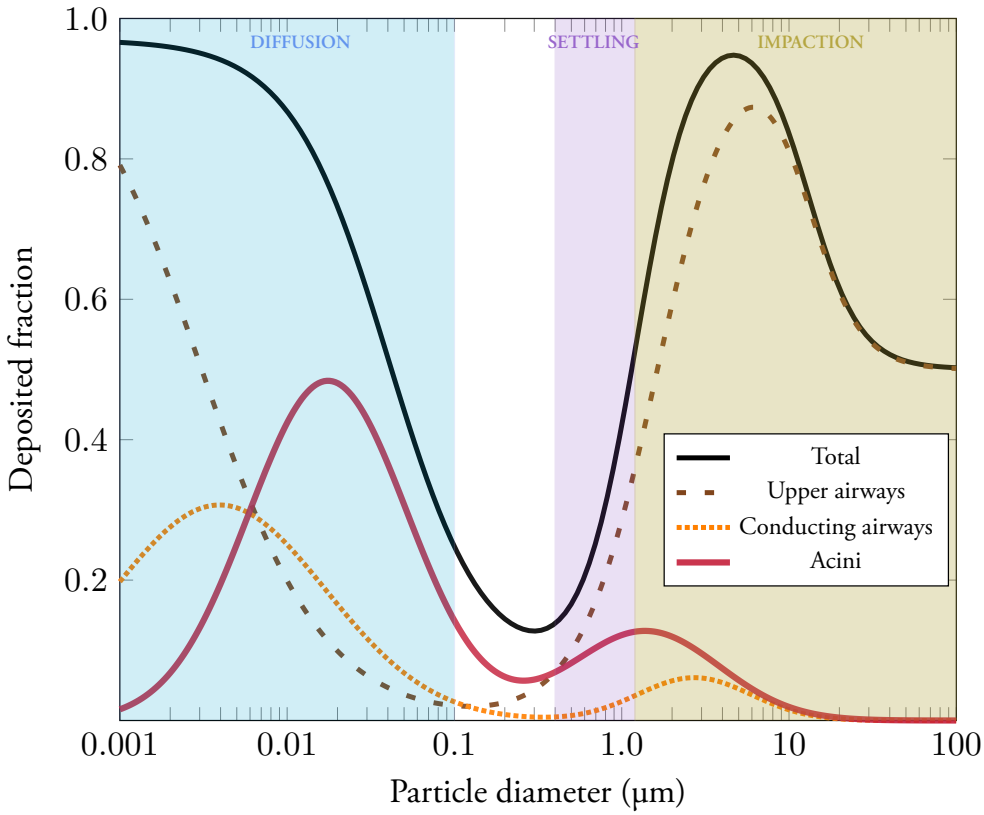

Figure 3: Deposited fractions of inhaled particles as a function of particle diameter, for particles with diameters between 1 nm and 100 µm. The curves come from equations that approximate the International Commission on Radiological Protection (ICRP) model for respiratory tract particle deposition. Equations are from Hinds (1999). Color shading indicates the dominant deposition mechanisms for the different particle sizes.

spherical unit density particles during one complete breath. They represent average values for males and females at three levels of physical activity.

The curves describing regional deposition reflect the strong particle size dependence, local respiratory tract geometry and airflows therein. Particle deposition is low for particle sizes 0.1 to 1 µm. Total deposition is high at both ends of the particle size range from 10 nm to 100 µm. For particle sizes above 1 µm, gravitational settling and impaction are the dominant deposition mechanisms. For particles with diameters below 0.1 µm, diffusional deposition is the primary deposition mechanism.

Inertial impaction and interception

Particles deposit by inertial impaction due to their inability to follow curvilinear airflows. Particles larger than a few micrometres in diameter efficiently deposit due to impaction in the upper airways and the first generation of the conducting airways where the airflows are high. The primary sites for the deposition of these particles are at the carinal ridges of the airway bifurcations. Interception occurs when a particle follows a streamline close to an airway wall such that the particle will adhere to the airway wall.

Gravitational settling

Particles that settle due to gravitational forces quickly reach settling velocity. Particles with d_p ~1 µm that pass through the upper airways efficiently deposit by gravitational settling in the conducting airways. If the particles reach the acini, they can have enough time for gravitational settling.

Diffusional deposition

Deposition by Brownian diffusion, governed by diffusivity (Equation 2), is most efficient in the distal lung where the airspaces are small, residence time relatively long and flow velocities low. A significant portion of fine and ultrafine particles that reach the acini will deposit there. Because of high airflow and high diffusion coefficients, ultrafine particles (in particular particles with d_p <10 nm) also deposit efficiently in the upper airways.

Ultrafine particle lung deposition changes due to respiratory disease

Since inhaled particle deposition probability depends on lung structure and airflows in the lungs, alterations to these factors can change the deposition of inhaled ultrafine particles. However, the experimental data on ultrafine particle deposition in individuals with respiratory diseases are scarce and the results inconsistent.

Studies with asthmatics have shown that the total deposited fraction of inhaled ultrafine particles was increased among asthmatics compared to healthy subjects (Olvera et al., 2012; Chalupa et al., 2004). The results were attributed to increased diffusional losses due to enhanced ventilation and hyperinflation of airways in asthmatics, compared to healthy individuals.

Studies conducted to measure inhaled ultrafine particle deposition in subjects with COPD have identified differences in the deposited fraction between subjects with COPD and healthy subjects (Anderson et al., 1990; Brown et al., 2002; Moller et al., 2008; Löndahl

et al., 2012). However, the deviations between COPD patients and controls were both that more ultrafine particles deposited in subjects with COPD as compared to controls (Anderson et al., 1990; Moller et al., 2008) and the opposite (Brown et al., 2002; Löndahl et al., 2012).

The discrepancies can be attributed to differences between experimental setups, different particle types used, and the differences in breathing maneuvers implemented: spontaneous breathing (Brown et al., 2002; Löndahl et al., 2012), controlled breathing airflow (Anderson et al., 1990) or the inhalation of a bolus (Moller et al., 2008). Also, the disease states of the participants in the studies were classified with different diagnostic tools. Moreover, the group differences identified are uncertain due to low sample sizes, typically with 3-10 subjects with COPD in each group (Anderson et al., 1990; Brown et al., 2002; Moller et al., 2008; Löndahl et al., 2014, 2017).

Particle clearance

Inhaled particles are cleared from the respiratory tract by four main mechanisms: (1) via the mucociliary escalator, (2) phagocytosis by macrophages, (3) entry to the lymphatic system, and (4) through absorption into the blood circulation. In the upper and conducting airways, the mucociliary escalator carries deposited particles to the pharynx by the repeated beating of the underlying cilia that make the mucus continuously move towards the pharynx. Alveolar macrophages engulf, and transport deposited particles in the acini to the mucociliary escalator or to the lymphatic system. Deposited particles can enter the lymphatic system and remain there for a long time. Translocation, in the form of dissolution and absorption into the bloodstream, takes place in all regions of the respiratory tract except in the anterior nasal passages. Dissolved material can penetrate through epithelial cells or pass between them. The rate of absorption differs from region to region depending mainly on thickness of the epithelial cells (Wang, 2005).

Models of particle deposition

The current understanding of respiratory tract particle deposition comes from a combination of experimental results and numerical predictions. All such models make simplifying assumptions about lung geometry and use theoretical or empirical equations to calculate particle deposition in different regions of the respiratory tract.

In general, the primary difference between the various whole lung particle deposition models is the choice of lung model. With increasing complexity of the lung model comes increasing computational costs. The models that are computationally most convenient are based on the assumption that a measured fraction of the airways is representative of the full

lung. Examples of such lung models are the International Commission on Radiological Protection (ICRP) model (Smith, 1994) , the Weibel model (Weibel, 2017) and the Yeh& Schum mode (Yeh and Schum, 1980) . In these symmetrically branching deterministic lung models, the airways in each generation have identical linear dimensions and consequently, all pathways of inhaled particles are identical during inhalation and exhalation (Hofmann, 2011).

Deterministic asymmetric models, also referred to as multiple-path models, consider the asymmetric airway branching pattern. Full asymmetric stochastic multiple-path models account for many varying variables, including airway dimensions, branching angles, and acinar volume, which gives highly variable path-lengths from trachea to a given generation (Asgharian et al., 2001). Respiratory physiology, airflow patterns and deposition mechanisms are other parameters that are treated differently in the models.

Two of the most employed models are the ICRP and the National Council on Radiation Protection and Measurements (NCRP, 1997) models. They are both based on a combination of experimental and analytical solutions to predict regional deposition. The deterministic multiple path particle dosimetry (MPPD) model (Asgharian et al., 2001) was developed based on the stochastic model first proposed by Koblinger and Hofmann (1990).

Respiratory tract particle deposition is generally modeled with input values for tidal volume (V_t) and breathing cycle (T_{bc}) to represent the breathing pattern, while FRC is used to scale the lung model. One exception to this is the parametrization described by Kim and Hu (Kim and Hu, 2006), which take V_t and T_{bc} as input variables, but not FRC. Particle characteristics are also used as input in the models.

Distal airspace radius from nanoparticle lung deposition

Several attempts have been made to use particle lung deposition with micron-sized particles to estimate the sizes of airways and airspaces in human lungs (Blanchard, 1996b; Bennett and Smaldone, 1988; Blanchard, 1996a; Brand et al., 1995; Gebhart et al., 1981; Lapp et al., 1975; Palmes, 1968, 1973). The rationale behind these methods is the same as for AiDA: an inhaled particle that has reached the lung, will remain airborne until it has traversed a distance necessary to strike a wall. The distance that a particle moves to reach an airspace wall is determined by the size of that airspace. Therefore, the number of aerosol particles that is still airborne, after a breath-hold time, provides an index for the size of the airspace containing the aerosol during the breath-hold. Based on measuring the number of recovered particles and particle lung residence time (t_{res}), conclusions are drawn on the size of the airspaces.

The advantages of using nanoparticles over micron-sized particles are mainly that: 1) nano-

particles penetrate deeper into the lungs without too great dependence on breathing airflow, and 2) nanoparticles diffuse faster than micron-sized particles, so that diffusion is the main deposition mechanism (Löndahl et al., 2017).

The theory behind estimating airspace size from diffusional losses in the lungs is based on solving the diffusion equation in circular tubes (Goldberg and Smith, 1981; Yu et al., 1977). The solution is used to find an expression for the particle concentration that remains airborne after a time t: $R(t)$, here referred to as the recovery. Assuming axisymmetric boundary conditions and a homogenous initial particle concentration in a cylinder with radius r, the recovery $R(t)$ of particles after a time t is given by

$$R(t) = 4\sum_{n=1}^{\infty} \frac{1}{k_{0,n}^2} e^{-\frac{k_{0,\mathrm{n}}^2 Dt}{r^2}},$$

where $k_{0,n}$ is the nth root of the Bessel function of the first kind ($J_0(x)$=0) and D the diffusivity given by Equation 2. For particles with d_p <100 nm, the expression will be dominated by the first exponential in the sum (corresponding to n=1) after only a few seconds. The $R(t)$ can therefore be approximated by a single exponential decay:

$$R(t) = R_0 e^{-\frac{k_{0,1}^2 Dt}{r^2}}, \tag{4}$$

where R_0 is the particle recovery at t=0. For the particle half-life time in the lungs ($t_{1/2}$) an expression for the cylinder radius r can then be found:

$$r = \left(\frac{k_{0,1}^2 D t_{1/2}}{\ln(2)}\right) = 2.89\left(D t_{1/2}\right)^{1/2}, \tag{5}$$

where the $k_{0,1}$=2.41 has been used to get the r.h.s of Equation 5. When measuring particle recovery from a collection of cylinders, the half-life time $t_{1/2}$ is associated with the diffusional loss in all cylinders. Therefore, the radius r in Equation 5 corresponds to an rms radii for a collection of cylinders, each with an individual radii r_i. This becomes apparent when rewriting Equation 5 in the following way:

$$r = 2.89\left(D t_{1/2}\right)^{1/2} = 2.89\left(D\frac{1}{m}\sum_{\mathrm{i}=1}^{m} t_{1/2,i}\right)^{1/2} = \left(\frac{1}{m}\sum_{\mathrm{i}=1}^{m} r_i^2\right)^{1/2}. \tag{6}$$

In consequence, r is weighted towards larger r_i. From here on forward, r in Equation 5 will be referred to as r_{AiDA} and is assumed to corresponds to an rms airspace radius in the distal lung. For the recovery data collected in this work, R_0 and $t_{1/2}$ were estimated and Equation 5 was used to calculate r_{AiDA} from the $t_{1/2}$.

2.3 Lung function and structure measurements

Lung volumes

The volumes of inspired, expired, and residual gas in the lungs at different points during tidal breathing, and at extremes of inspiration and expiration, provide crucial information for describing lung structure and function. Such measurements also provide reference points for quantitative measurements. Table 2 and Figure 4 present written and pictorial descriptions of lung volumes that are important in routine clinical practice.

For an average human adult, TLC is about 6-7 L while RV is about 20-30% of TLC and increases with age. At normal tidal breathing, the TV is about 0.45-0.60 L but can reach up to about 3 times more during physical exercise. FRC is determined by the balance between the inward recoil of the lungs and the outward recoil of chest walls and is about 2-3.5 L for a healthy adult. Relaxation of the muscles allows the lungs to recoil, but at the end of maximum exhalation, RV is still left in the lungs and cannot be expelled, mainly due to small airway collapse and the stiffness of the chest. The respiratory volumes and capacities can differ considerably between adults, and between healthy individuals and patients with lung disease.

Table 2: Lung volume and capacity descriptions with acronyms.

Lung volume/capacity	Description
Tidal volumne (TV/V_t)	Peak-to-peak inspiratory-to-expiratory volume during normal tidal breathing
Inspiratory reserve volume (IRV)	Volume of air beyond TV that can be inspired
Expiratory reserve volume (ERV)	Volume of air beyond TV that can be expired
Residual volume (RV)	Volume of air in the lungs after maximal exhalation
Forced expiratory volume in 1 second (FEV_1)	The volume of air that can be forcibly expired in 1 s
Total lung capacity (TLC)	The volume of air that can be contained in the lungs
Inspiratory capacity (IC)	Volume of air that can be inspired from tidal exhalation
Vital capacity (VC)	The volume inspired when TLC is achieved (VC=TLC-RV)
Functional residual capacity (FRC)	Volume of air remaining in the lungs after tidal exhalation

Standard pulmonary function tests

Pulmonary function tests (PFTs) include a range of measurement techniques that involve breathing air or specific tracer gases to probe aspects of lung physiology. The resulting PFT values are generally reported in comparison to predicted values for a given subject. These predicted values are derived from empirical reference equations for healthy subjects with equivalent background characteristics (including age, sex, height, ethnicity).

The measurements of static and dynamic lung volumes provide information about the lungs' mechanical properties but do not quantify the gas exchange. The spirometry test

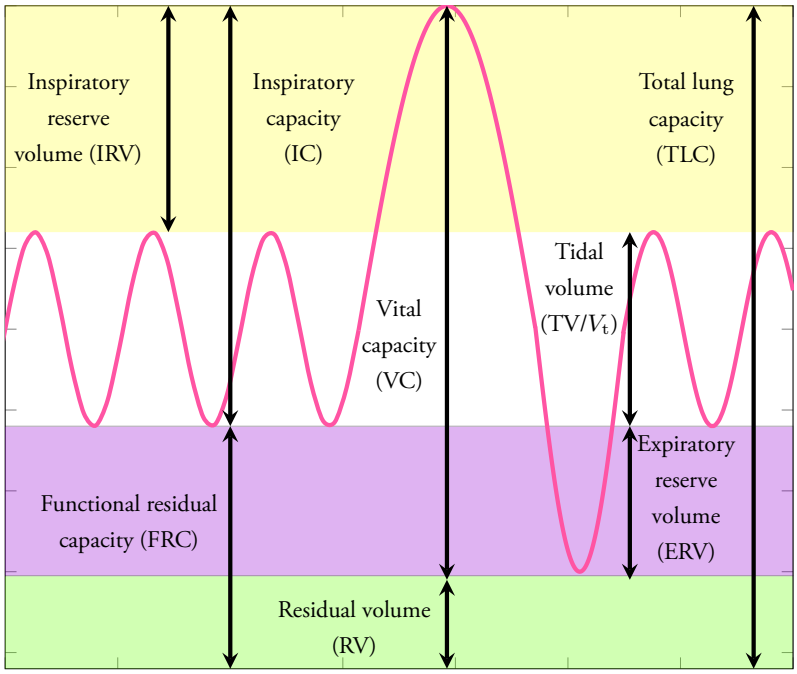

Figure 4: Diagram of lung volumes achieved during steady tidal breathing followed by forced inhalation and forced exhalation. All lung volumes and capacities, except FEV_1, are displayed.

is performed by instructing the subject to inhale to maximum after a period of tidal breathing and then exhale to his/her full capacity for measurement of dynamic lung volumes. Spirometry, including the measurement of FEV_1 and VC, and their ratio (FEV_1/VC), is the most performed subset of PFTs. The measurements are used routinely to detect airflow obstruction for the diagnosis of various pulmonary disorders. COPD is commonly classified as FEV_1/VC (in % predicted) $<70\%$ (Celli et al., 2004). Globally, the most used spirometry measure is forced vital capacity (FVC), instead of slow vital capacity (SVC), but it has been shown that the use of FVC instead of SVC or VC may result in a considerable under diagnosis of airflow obstruction (Torén et al., 2016).

Due to the low contribution of distal lung obstruction to total lung resistance, it is very difficult to detect and dismantle changes in the distal lung with spirometry, unless the disease has advanced to a high degree. The measurements of the static volumes of TLC, FRC and RV, are rather insensitive to distal lung obstruction, and require additional techniques such as body plethysmography (Criée et al., 2011).

The lungs' ability to exchange gas can be quantified by performing a pulmonary function test to determine the diffusion capacity of the lung for carbon monoxide (D_{LCO}). For D_{LCO} measurements, a volume of gas containing carbon monoxide (CO) is inhaled until

TLC is reached, breath-hold is maintained for a few seconds and then the gas is expired. The inhaled and exhaled CO concentrations are recorded while the alveolar volume containing CO is inferred from the concentration of an insoluble tracer gas introduced in the CO gas mixture. A decreased D_{LCO} value in combination with airflow obstruction can indicate the presence of emphysematous changes in the lung, and the method can be used to study the progression of the disease. In practice, CO transfer is limited by the finite reaction rate of CO and hemoglobin (Marrades et al., 1997) and CO saturation of the blood.

In clinical practice, emphysema is diagnosed by traditional PFTs, medical history and physical examination. However, PFTs are reported to have low sensitivity for diagnosing early stage emphysema (Gurney et al., 1992).

Oscillometry

Mechanical features of the respiratory system can also be measured indirectly as the flow response to applied pressure impulses in the form of respiratory system impedance (Z_{rs}), from which respiratory resistance (R_{rs}) and reactance (X_{rs}) are derived. The measurements are referred to as oscillometry. To measure impedance, pressure impulses with varying frequencies are superimposed on normal tidal breathing while the change in pressure and flow is measured.

Resistance measured with relatively high frequency (20 Hz) impulses (R_{20}) is assumed to reflect proximal airways, while a lower frequency (5 Hz) resistance (R_5) reflects the full respiratory tract resistance. The difference between high and low frequency resistance (R_5-R_{20}) is thus proposed to reflect resistance in the distal lung. Reactance at low frequencies (X_5) supposedly reflects distal lung elasticity and lung heterogeneity. Both R_5 and X_5 have been identified to be abnormal in smokers with mainly normal spirometry (Faria et al., 2009, 2010; Jetmalani et al., 2018; Shinke et al., 2013). Patients with diagnosed COPD had significantly higher R_{rs} and lower reactance X_{rs}, compared to healthy subjects (Crim et al., 2011) and the changes have been related to the degree of airflow obstruction (Di Mango et al., 2006).

Oscillometry is scarcely used in pulmonary function testing, but it can potentially convey information about the distal lung and has good potential to be employed in pulmonary healthcare due to the minimal demand on subjects' performance. More data are still needed to assess how oscillometry provides additional information on the pathophysiology of COPD and other lung diseases (Kaminsky et al., 2022), and it is still debatable what airway generations R_5-R_{20} reflects.

Lung densitometry with computed tomography

The assessment of lung structure with computed tomography (CT) densitometry relies on the fact that X-ray attenuation is indicative of tissue density. Densitometry measurements are made on 3D cross-sectional images by rotating the X-ray source around the object that is imaged, followed by post-processing for quantitative voxel-by-voxel assessment of tissue attenuation value, measured in Hounsfield (HU) (Stolk and Stoel, 2011).

CT densitometry indices are based on the overall voxel attenuation distribution. The 15th percentile point is defined as the cut-off value, below which 15% of the voxels with lowest attenuation are distributed. The index is converted to the 15th percentile lung density (PD_{15}) in g/L by the addition of 1000 HU. The low attenuation volume (LAV) densitometry index is defined as the percentage of voxels with a HU value below a certain threshold. CT-derived total lung capacity (CT-TLC) can be calculated as the volumetric sum of all voxels containing lung tissue (Iwano et al., 2009).

A high prevalence of low attenuation is associated with a lower lung tissue density, for instance by emphysema. However, the resolution in CT is not enough to directly visualize distal lung structures. With CT there is always a dose of ionizing radiation required which limits its usage to monitor lung disease.

Distal lung structure measurements with diffusion-weighted magnetic resonance imaging

Conventional pulmonary magnetic resonance imaging (MRI) involves non-ionizing radio frequency (RF) radiation excitation and detection of the nuclear spin procession of protons (hydrogen nuclei ^{1}H) in the lungs, in a strong and stable homogenous magnetic field. Image contrast is provided by the lung tissue, including proton density, and magnetic resonance (MR) signal relaxation times. ^{1}H MRI of lungs is challenging due to the low proton density and magnetic susceptibility posted by air-tissue interfaces in the lungs.

To overcome this, lung MRI methods with hyperpolarized noble gases, helium-3 (^{3}He) and xenon-129 (^{129}Xe), have been established alongside ^{1}H lung MRI. For a sufficient signal-to-noise ratio for MRI acquisition, the low spin density of noble gases requires signal enhancement by hyperpolarization with spin exchange optical pumping. This allows the MRI signal to be increased 4-5 orders of magnitude. Diffusion-weighted (DW) MRI, where a varying field gradient (b) is introduced, enables evaluation of the apparent diffusion coefficient (ADC) of the hyperpolarized gas in the lungs.

Gas ADC is reduced when compared to its free diffusion coefficient due to the restriction imposed by airspace walls. Hence, in the presence of tissue destruction (e.g., emphysematous changes) ADC increases because the diffusion is less restricted, when compared to in a

healthy lung (Saam et al., 2000). The ADC can be calculated assuming a mono-exponential fit for the gas diffusion signal between b=0 (S_0) and b (S_b):

$$\mathrm{ADC} = \ln\frac{S_0/S_\mathrm{b}}{b}$$

^{129}Xe ADC mapping can be used for the assessment of COPD (Kaushik et al., 2011). ^{3}He and ^{129}Xe DW-MRI measurements have been shown to agree in healthy subjects and COPD patients Kirby et al. (2012, 2014). Although ^{3}He has a higher signal (due to higher gyromagnetic ratio), it is not naturally abundant, subject to regulations and expensive, while ^{129}Xe is naturally abundant and commercially available.

Several models that relate ADC mapping to distal lung structure have been validated with morphometric measurements with lung specimen (Woods et al., 2006; Yablonskiy et al., 2009). One such model is the stretched-exponential model (SEM) of hyperpolarized gas diffusion in the lungs (Chan et al., 2018). With the SEM, an expression for the mean diffusive length scale (Lm_D), a metric of mean free path in the distal lung, is derived. The method relies on fitting the hyperpolarized gas signal from the applied b-values to a stretched exponential fit:

$$\frac{S_\mathrm{b}}{S_0} = \int_0^\infty p(D)e^{-bD}dD = e^{(-bDDC)^\alpha}$$

where $p(D)$ is the probability distribution of different apparent diffusivities, DDC is the distributed diffusivity coefficient, and α the heterogeneity index describing the deviation from a mono-exponential fit. From the fit, the DDC and α are estimated, and a numerical expression for $p(D)$ can be found (Berberan-Santos et al., 2005). The mean diffusive length scale, Lm_D, is defined as the expectation value of $p(D)$ and the distribution of the characteristic diffusion lengths L_D:

$$L_m = \int_0^\infty L_D p(D)dD$$

where $L_D = \sqrt{2\Delta D}$ is the characteristic diffusion length for different apparent diffusivities and Δ the diffusion time. The Lm_D measured with ^{129}Xe DW-MRI has been shown to be in good agreement with realistic models of distal airway geometries (Chan et al., 2021). The α heterogeneity index has been found to be inversely related to increasing lung heterogeneity (Chan et al., 2021) and changes in the lung microstructure, while the DDC is dependent on diffusion time (Chan et al., 2019). DW-MRI testing has wide-ranging potential for measurement of distal lung structure (and function), but is due to its complexity and high cost only available in a few places in the world.

3 Methods

3.1 Studies overview

Nanoparticle lung deposition measurements were carried out with four different populations resulting in five different papers presented in this thesis. Table 3 outlines the study populations, selection criteria and lung measurements (in addition to AiDA) performed in the four studies.

In the **^{129}Xe DW-MRI-study**, the MRI measurements on all the participants were performed in Sheffield, UK. All other examinations were conducted at the hospital in Malmö, Sweden. Eight participants together had mean 7 ± 11 packyears (1 packyear = 20 cigarettes smoked per day for one year). The aim of the study was to benchmark the AiDA method against the ^{129}Xe DW-MRI measurements.

The **Swedish CArdioPulmonary bioImage Study (SCAPIS)** is a nation-wide population-based cohort with the overall aim to develop methods for the prediction and prevention of cardiovascular and pulmonary diseases. In SCAPIS in Malmö, Sweden, 744 participants were examined with the AiDA method. The results from a sub-group (N=618) are reported in Paper I, while the results from the full study population that passed the data quality checks (N=695) are presented in Paper III. Of the 695 subjects that passed the data quality checks, 103 participants reported that they were current smokers, and 420 (including both ex-smokers and current smokers) subjects collectively reported the mean of 17 ± 13 packyears.

For the **Welders study**, welders employed at two different companies in the southern Sweden were recruited for the study presented in Paper IV. The controls in the study worked in offices or at the hospital. Among the welders 1 smoked and 14 were ex-smokers, with a collective mean of 11 ± 15 packyears. Two controls were ex-smokers with mean 16 ± 10 packyears. The aim of the study was to test if we could detect lung changes in welders compared to controls by using new sensitive methods.

In the **Befdos-study**, particle lung deposition measurements with 2 µm particles were performed, as well as AiDA measurements and lung function examinations. The aim was to evaluate particle deposition models with experimental data, and then go on to identity variations that explained respiratory tract particle deposition, and the differences between the modeled and measured total lung deposition.

Table 3: Study populations, selection criteria and lung measurements performed in addition to the AiDA-measurements in each study.

Study	N	N_f	M/F	Age range (years)	Selection criteria	Measurements	Paper
^{129}Xe DW-MRI	25	23	14/9	23-70	Healthy No previous lung disease	^{129}Xe DW-MRI Spirometry Plethysmography D_{LCO}	I
SCAPIS	744	695	328/367	50-64	Population-based	Spirometry D_{LCO} Oscillometry D_{LCO} CT	II& III
Welders	45	44	44/0	27-73	Healthy Non-smoking No previous lung disease	Spirometry Oscillometry D_{LCO}	IV
Befdos	17	17	9/8	22-67	Healthy No previous lung disease	Spirometry Oscillometry Plethysmography D_{LCO} 2 µm particle deposition measurements	V
Total		779	395/384	22-70			

N: number of participants, N_f: number of participants with complete and quality checked data,
M: number of male subjects, F: number of female subjects.

3.2 Nanoparticle lung deposition measurements

The nanoparticle lung deposition measurements were performed to measure particle recovery from the distal lung. From the breathing pattern of each measurement, particle lung residence time t_{res} was extracted. Particle half-life time $t_{1/2}$ and zero seconds recovery R_0 were determined from measured recovery dependency on t_{res}. Equation 5 was used to calculate r_{AiDA} based on the extracted $t_{1/2}$.

The setup

The nanoparticle lung deposition setup is extensively described in other publications (Jakobsson et al., 2016, 2018a). The setup followed the experimental guidelines for lung deposition measurements described in (Löndahl et al., 2014). Figure 5 presents a schematic graphic of the setup. Monodisperse 50 nm hydrophobic polystyrene (PS) nanoparticles were aer-

osolized with an electrospray aerosol generator (Model 3480, TSI Inc.). Particles passed a neutralizer and were size-selected with a differential mobility analyzer (DMA, Model 3071, TSI Inc.). Generated particles were diluted with particle-free air in a flexible antistatic reservoir. A computer-controlled valve directed the aerosol to a mouthpiece and exhaled particles into a sample collector consisting of a 1-m metal tube 35 mm in diameter. The system was heated to body temperature and constructed in electrically conducting material to limit condensate formation and electrostatic particle losses, respectively. The breathing pattern was recorded with a pneumotachograph flowmeter close to the mouthpiece. Inhaled and exhaled particles were sampled at a frequency of 1 Hz and with a flow of 1 $Lmin^{-1}$, with the same particle condensation counter (CPC; Model a20 Airmodus) after drying the aerosol with a Nafion single-tube drier (Perma Pure, Toms River, NJ, USA).

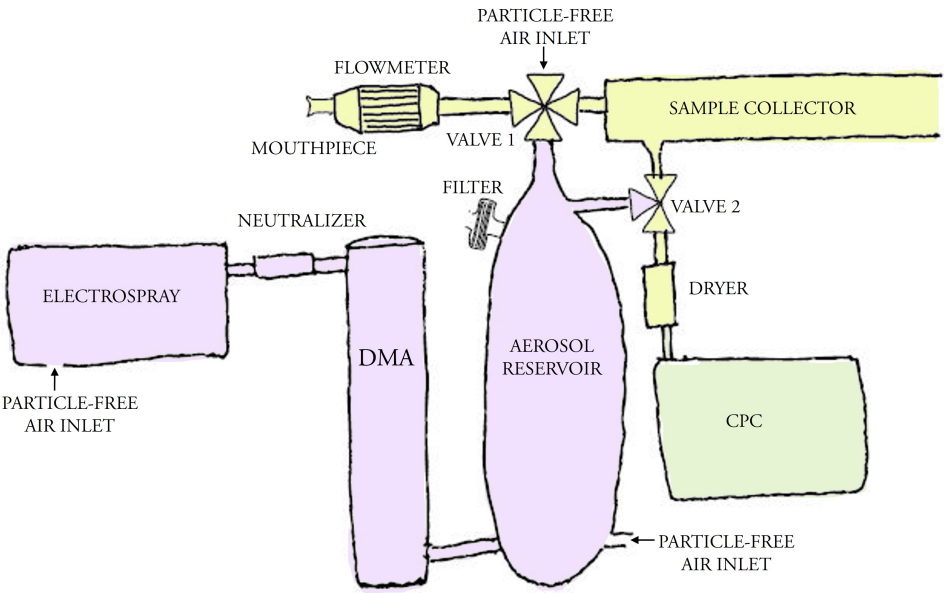

Figure 5: Schematic diagram of the AiDA setup. The aerosol generation system (purple) consisted of an electrospray aerosol generator, a differential mobility analyzer (DMA) for particle size selection and supply of particle free air for dilution. The inhalation and sampling system (yellow) consisted of a pneumotachograph flowmeter, a computer controlled valve and a sample collector. To avoid condensation, the inhalation system were heated to body temperature. Inhaled and exhaled particle concentrations were quantified with a condensation particle counter (CPC).

Lung deposition measurements

Duplicate recovery measurements were performed for each breath-hold time between 5 and 15 seconds. A nose-clip was used to assure that the subject only breathed through the mouth. Figure 6 display example data from one lung deposition measurement: the breathing pattern and the particle concentrations measured.

Figure 6A illustrates the breathing procedure performed for each particle lung deposition measurement with four points (1-4) marked with green arrows. At the beginning of each measurements the subject breathed particle-free air for at least 30 seconds. Next, the subject exhaled to RV (point 1 in Figure 6A) followed by a fast inhalation to TLC from the aerosol reservoir (point 1 to 2). After the complete inhalation, the subject held his/her their breath for a predefined time. After the breath-hold time the subject exhaled 1300 mL into the sample collector (point 3 to 4). When 1300 mL had been exhaled, the valve closed and the remaining exhalation was directed outside the sample collector. Prior to the inhalation maneuver, the CPC measured the particle concentration from the aerosol reservoir. Once 1300 mL had been exhaled, the CPC measured the concentration from the sample collector.

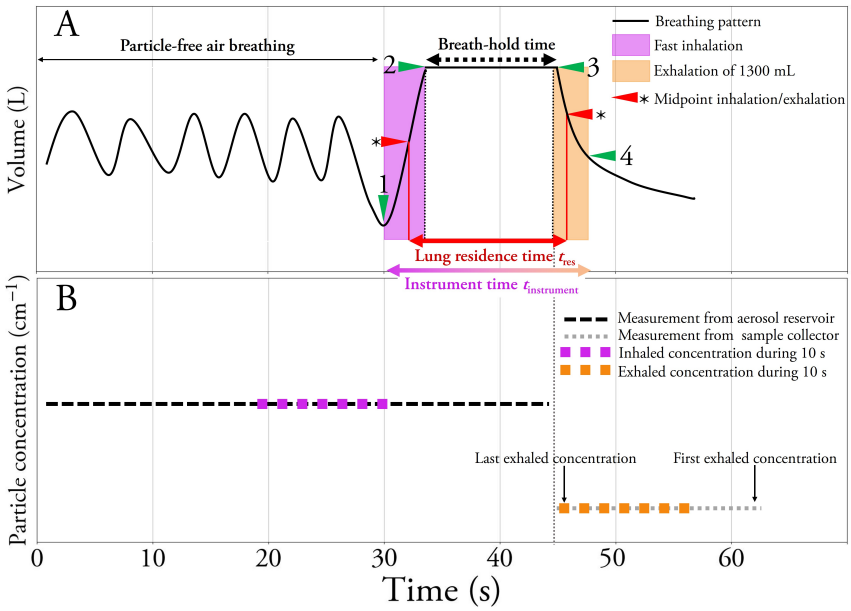

Figure 6: An exemple of AiDA data: breathing pattern (A) and particle concentrations (B) recorded during one particle lung measurement.

As seen in Figure 5, the CPC measured particle concentrations from the part of the sample collector closest to the mouthpiece. In consequence, the first measured particle concentration came from the deepest part of the lung. Figure 6B display example particle concentrations measured with the CPC. The inhaled and exhaled particle concentrations were measured during 10 seconds, from the aerosol reservoir and the sample collector, respectively.

The average inhaled concentration was between 1800 and 7000 cm^{-3}. Assuming a VC of about 3 L for one full breath of the particle concentration 7000 cm^{-3}, approximately 20 million particles were inhaled in each particle deposition measurement. Consequently,

about one nanoparticle reached and deposited in 5% of all alveoli, in each measurement. The mean total deposited fraction was 80-90%, corresponding to recoveries of about 10-20%.

In the Befdos study (Paper V), additional AiDA-measurements were performed with particle deposition at a shallower volumetric lung depth, approximated to be half the inhalation volume of a standard AiDA measurement. In these measurements, after the 30 s of initial breathing of particle-free air, the subject inhaled nanoparticles to half VC, instead of VC. Hence, the volume between points 1 and 2 in Figure 6A, was about half he volume of the other AiDA measurements. The volume approximating half VC for these measurements was measured with spirometry.

Analysis of lung deposition data

Data quality checks

Data quality checks were performed for the breathing pattern and the measured particle concentrations before the analyses to extract airspace radius, r_{AiDA}, and zero seconds recovery, R_0 . Data quality requirements are listed in Table 4. Data were excluded if the requirements were not fulfilled. Data that did not fulfill requirements 1-3 were excluded prior to further analyses, while requirements 4-5 were checked in the last step of the analysis, prior to estimating R_0 and calculating r_{AiDA}.

Table 4: AiDA data requirements

Characteristic		Requirement
Inhaled volume	1	$>$ 1300 mL
Inhaled concentration	2	$>$ 1000 cm^{-3}
Stable inhaled concentration	3	Deviation $<$ 10%
Number of measurements	4	At least 4 recovery measurements passing requirements 1-3
Fit	5	R^2>0.85

R^2: coefficient of determination

The particle deposition data analysis was performed in three steps: (1) estimation of lung residence time from the breathing pattern, (2) calculation of distal lung particle recovery from measured particle concentrations, and (3) extraction of half-life time of particles in the distal lung. Steps (1) and (2) were performed for all recovery measurements, prior to step (3).

Analysis of breathing patterns

Particle residence time t_{res} in the lungs was defined as the midpoint between inhalation and exhalation, indicated by red arrows with asterisks in the breathing pattern shown in Figure 6A. To identify these midpoints, points 1-4 were first identified.

An algorithm was developed to analyze all breathing-patterns and identify the points 1-4 outlined in Figure 6A. The four points were identified by dividing the breathing pattern into segments based on the valves opening and closing times. Point 1 was identified as the lowest point in the breathing pattern for the time gap when the aerosol reservoir was open. The plateau in the breathing pattern was determined as the time-range during which the time-derivative of the breathing pattern was zero. Points 2 and 3 were identified as the starting and ending points of this segment. Point 4 was identified as the point after which 1300 mL had been exhaled from point 3. The difference in volume between points 1 and 2 was the total volume inhaled.

The inhalation midpoint was identified as the time at which half the total volume had been inhaled (midpoint between points 1 and 2). The exhalation midpoint was identified as the point at which 650 mL had been exhaled (midpoint between points 3 and 4). Lung residence time, t_{res}, was determined as the total time that elapsed between inhalation and exhalation midpoints. The total inhaled volume V_{tot} of aerosol was the volume between points 1 and 2. The time the particles spent in the instrument, $t_{\mathrm{instrument}}$, was the time between points 1 and 4 minus the breath-hold time.

Particle recovery from the distal lung

The inhaled particle concentration (C_{in}) was estimated to be the mean particle concentration measured during 10 seconds prior to the subject exhaling to RV (point 1 in Figure 6A). Exhaled particle concentration (C_{ex}) was taken to be the mean particle concentration measured over the 10 seconds after 1300 mL had been exhaled. Inhaled and exhaled particle concentrations were thus measured on 160 ml of inhaled and exhaled volumes. Measured particle recovery R was calculated as the fraction between C_{ex} and C_{in}. No correlation between inhalation flow rate and recovery was observed.

To account for particle losses in the system, the calculated recovery, R, was multiplied by an empirically determined correction factor C, as described by (Jakobsson et al., 2016). The correction factor was a function of the time that particles spent in the instrument, $t_{\mathrm{instrument}}$, and the total volume inhaled, V_{tot}, determined from the breathing pattern:

$$C = Ae^{B\frac{t_{\mathrm{instrument}}}{V_{\mathrm{tot}}}}, \tag{7}$$

where A=1.074 and B=0.22 had been experimentally determined for 50 nm particles. A linear least squares 1st order polynomial was fitted to the logarithm of the measured recovery R as a function of t_{res} (see Figure 7) on the form:

$$\ln(R) = \ln(R_0) + k \cdot t_{\text{res}}$$

The R_0 was extracted from the fit and half-life time ($t_{1/2}$) was calculated from the slope k:

$$t_{1/2} = \frac{\ln(1/2)}{k}$$

From Equation 5, r_{AiDA} was calculated based on $t_{1/2}$ and the diffusion coefficient D (Equation 2) for PS nanoparticles.

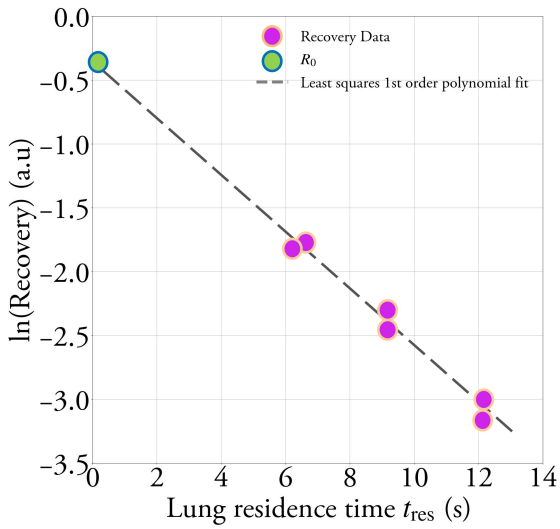

Figure 7: Measured recovery R as a function of lung residence time t_{res} from 6 recovery measurements with breath-holds 5, 7, and 10 seconds. R_0 and $t_{1/2}$ were extracted from the least squares line fitted to the data.

3.3 Clinical lung measurements

Standard pulmonary function tests and oscillometry

Spirometry, body plethysmography and D_{LCO} measurements were performed according to the American Thoracic Society and European Respiratory Society (ATS/ERS) standards. In all studies here presented, spirometry was performed 15-20 minutes after bronchodilation for measurement of VC and FEV_1. Respiratory impedance was measured with oscillometry

yielding measurements of total airway resistance R_5, proximal airway resistance R_{20}, small airway resistance R_5-R_{20}, and reactance X_5.

Computed tomography measurements

Generated X-ray images were evaluated by one of four chest radiologists in SCAPIS. CT-derived total lung capacity (CT-TLC) was calculated as the sum of all voxels containing lung tissue. The percentage of voxels with a HU value below -950 (LAV) was recorded. The four chest radiologists also assessed emphysema visually.

Hyperpolarized ^{129}Xe DW-MRI measurements

The ^{129}Xe DW-MRI measurements were performed with b = [0, 12, 20, 30 s cm^{-2}], with a 16 seconds breath-hold after an inhalation of 1L gas mixture containing 550 mL polarized ^{129}Xe and 450 mL N_2 from FRC. From the ADC measurements, the distributed diffusivity DDC, alpha heterogeneity index α and Lm_D were derived by application of the SEM model. Figure 8 presents examples of ^{129}Xe DW-MRI mean ADC measurements for one subject in the study.

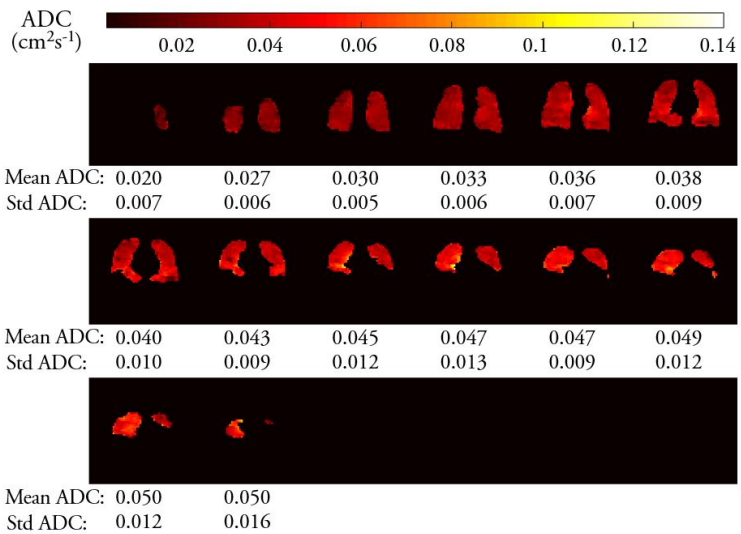

Figure 8: Example of mean ADC measurements from ^{129}Xe DW-MRI with b= 0, 12, 20, 30 s cm^{-2} in the study here presented. Image courtesy of POLARIS group, Sheffield University.

3.4 Other lung deposition measurements and modeling

Respiratory tract particle deposition was measured at spontaneous breathing with a setup similar to a previously used and described system (Löndahl 2006, Rissler 2012, Rissler 2017). Monodisperse 2 µm silicon dioxide particles, with geometric mean diameter 1.7 µm, corresponding to an aerodynamic diameter 2.3 µm, were generated with an atomizer. Particles were dried and diluted to a stable concentration of approximately 50 cm^{-3}. Inhaled and exhaled particle concentrations were measured in parallel using two aerodynamic particle sizers (APS, model 3321, TSI Inc.) after drying the aerosol. Breathing airflows were measured with a pneumotachograph to estimate tidal volume V_t and breath cycle time T_{bc}. A nose clip was used to assure breathing through the mouth only. Deposition measurements were performed by measuring inhaled and exhaled particle concentrations during three consecutive 5-minute periods, a total deposited fraction (DF) was calculated as the average for each measurement period.

The total deposited respiratory tract deposition was modeled using the MPPD, ICRP and NCRP with input parameters V_t, T_{bc} and FRC, and with the parameterisation suggested by (K&H, Kim and Hu, 2006), with input parameters V_t and T_{bc}. The MPPD model was implement with two different lung anatomy models: the asymmetric Pacific Northwest National Laboratory (PNNL) model and the Yeh and Schum model (Y&S, Yeh and Schum, 1980). MPPD is freely available online, while ICRP and NCRP were implemented with Preludium Mimetikos PreludiumTM v1.2.0.0 (Olsson and Bäckman, 2018).

3.5 Ethical considerations

Ethical approvals were obtained from the Regional Ethics Committee at Lund University (2018/659 Paper I; 2016/1031 Paper II & III; 2018/361) and from the Swedish Ethical Review Authority (Paper IV; 2019/04770 Paper V), in accordance with the Declaration of Helsinki.

Detailed oral and written information about the purposes of the studies were formulated and given to all participants. All subjects participated voluntarily in the studies. The participants were ensured that they could stop their participation at any time. Signed consent was obtained from all participants at the start of each study. Data protection, privacy and confidentiality of personal data collected and processed were handled in accordance with EU legislation. The participants' identities will not be revealed at any stage of the research projects.

All studies contained lung measurements which were evaluated by medical doctors. If abnormal values or quantities appeared, the subjects were contacted by the medical personnel for follow-up examinations, and possible treatment of conditions.

The exposure to nanoparticle concentrations during the AiDA measurements, and in the other lung deposition measurements, were comparable to or lower than normal urban air particle concentrations. Nanoparticles are ubiquitous in ambient air. In urban European settings the everyday particle number concentrations are on average on the order of 10^{3} - 10^{4} cm $^{-3}$ (Ketzel et al., 2003; Longley et al., 2004). Assuming a mean deposition probability of 0.5, such concentrations result in a corresponding approximate dose of 10^{11} particles delivered to the distal lung per day. In comparison, the approximate 20 million nanoparticles deposited in the distal lung during a lung deposition measurement can be considered low. The cumulative exposure to particles in six consecutive measurements can also be considered low due to the inhalation of clean particle-free air prior to each measurement. For a total of six particle deposition measurements, the total mass of particles delivered to the lung was below 3 µg. This can be compared to an everyday cumulative dose above 10 µg due to ultrafine particle exposure in European urban environments (Hussein et al., 2019; Kaur et al., 2005).

3.6 Statistical analysis

Means with associated standard deviations (SD) were used to describe reported values. Spearman's rank correlation (ρ) and Pearson's correlation coefficient (r) were used to determine associations between variables. A probability value (P-value) 0.05 was set to indicate the level of statistical significance. Pearson correlations were classified to be low in effect size for absolute values of r below or equal to 0.3, moderate between 0.3 and 0.7 and strong above 0.7.

The agreement between airspace radius r_{AiDA} and the Lm_D measured with DW-MRI was assessed with the Bland-Altman analysis. From this, a bias between mean differences and an agreement interval were identified. A principal components analysis (PCA) was performed to study the explained variance in SCAPIS. T-tests were used to assess significance of differences between groups.

4 Results

4.1 Benchmarking AiDA with ^{129}Xe-DW-MRI

The r_{AiDA} correlated significantly with hyperpolarised ^{129}Xe DW-MRI measured diffusion parameters: ADC, DDC, and mean diffusion length scale Lm_D (Table 5, Paper I). The group mean r_{AiDA} was measured to be 279±25 µm, while the mean Lm_D was 281±19 µm. The r_{AiDA} was linearly correlated with Lm_D with a slope of 1 and standard error 0.3 µm, according to a linear regression fit (Figure 9A). The Bland-Altman comparison between r_{AiDA} and Lm_D indicated that r_{AiDA} increased more than Lm_D, with increasing airspace size (r=0.5, P=0.01, Figure 9B). An average mean bias 1.2 µm towards r_{AiDA} was identified. Zero seconds recovery, R_0, decreased with increasing α heterogeneity (Figure 9C). No correlations were observed between AiDA indices and lung function measurements.

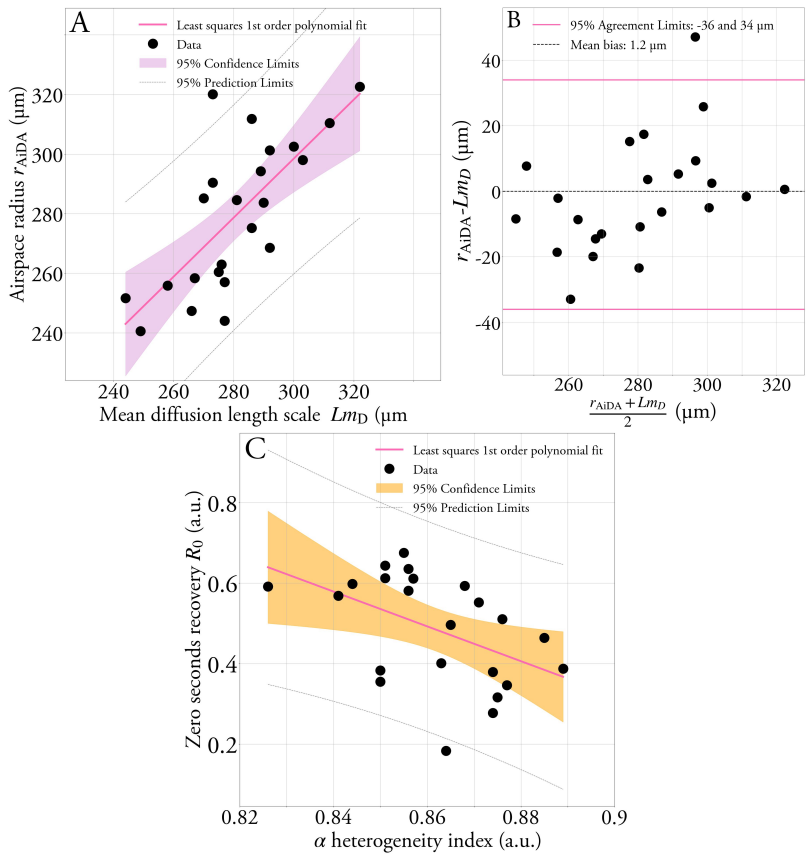

Figure 9: Airspace radii r_{AiDA} as a function of mean diffusion length scale Lm_D (A), Bland-Altman plot comparison between r_{AiDA} and Lm_D (B) and R_0 as a function of α heterogeneity index (C).

Table 5: Correlations and linear regression models for airspace radius r_{AiDA} with parameters for diffusion linear mean distance Lm_D, apparent diffusion coefficient ADC, distributed diffusivity coefficient DDC and for zero seconds recovery R_0 correlation with α heterogeneity parameter measured with DW-MRI. The linear regression models (slope, SE and P) were adjusted for height, weight, age and pack-years.

Comparison	r	P	ρ	P	Regression coefficient	SE	P
r_{AiDA} VS. Lm_D	0.71	<0.001	0.68	<0.001	1.0 (a.u)	0.3 µm	0.001
r_{AiDA} VS. ADC	0.75	<0.001	0.69	<0.005	0.5 (s cm^{-1})	1100 µm	<0.001
r_{AiDA} VS. DDC	0.73	<0.001	0.66	<0.005	0.5 (s cm^{-1})	1000 µm	<0.001
R_0 VS. α	-0.48	<0.02	-0.48	<0.02	-4 (a.u.)	2 (a.u.)	<0.001

r: Pearson's correlation coefficient, P: level of statistical significance, ρ: Spearman's rank correlation coefficient, SE: standard error.

4.2 The r_{AiDA} were on average larger in individuals with emphysema detected by CT

Individuals with emphysema detected with CT in SCAPIS had average larger r_{AiDA} compared to subjects that did not have emphysema according to CT (Paper II). In total, 57 subjects had emphysema according to visual judgement, 55 subjects had LAV>5% and 18 subjects hade LAV>7% (Table 6). For the individuals that had visually detected emphysema and LAV >5%, r_{AiDA} was significantly larger compared to the subjects that did not have emphysema according to the CT-assessment. With increasing r_{AiDA}, the number of subjects with emphysema increased (Figure 10), and lung function decreased as measured with $\mathrm{D_{LCO}}$ and spirometry (see Paper II). Both r_{AiDA} and R_0 were positively correlated with increasing LAV percentage and negatively correlated with $\mathrm{PD_{15}}$. However, in all cases the correlation effect size was low (see Paper III).

Table 6: Number of subjects with emphysema according to the different CT-assessment methods, mean $r_{\mathrm{AiDA}}\pm$SD and r_{AiDA} range among them, among subjects with no visually detected emphysema or LAV <5%, and in the full group of participants in the study

	N	Mean r_{AiDA} (µm)	r_{AiDA} range (µm)
Visually detected emphysema	57	328±50	258-580
LAV>5 %	55	319±54	227-580
LAV>7%	18	331±70	257-580
Subjects without visually detected emphysema and/or LAV<5%	625	283±37	200-445
The full group	695	287±40	200-580

4.3 AiDA indices explained variance in data that no other lung measurements explained

The AiDA indices were not consistently correlated with standard lung function measurements or oscillometry variables, neither for raw data measurements nor for percent pre-

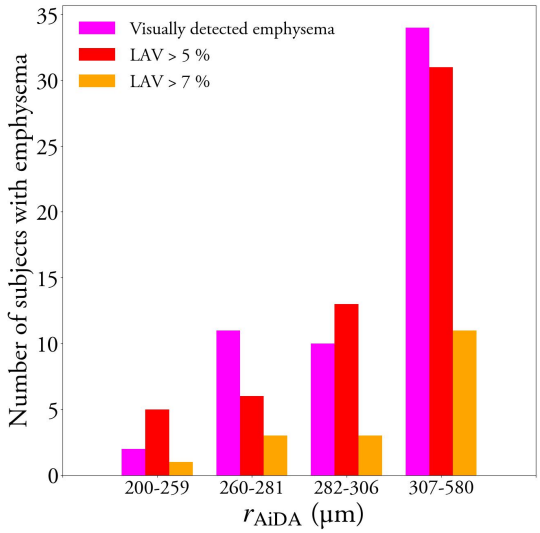

Figure 10: The number of participants with emphysema according to CT per r_{AiDA} quantile.

dicted values. The two AiDA indices were not correlated with each other.

The SCAPIS data gave rise to a positive correlation between r_{AiDA} and FEV_1/VC, and negative correlations for r_{AiDA} with VC, oscillometry variables and $\mathrm{D}_{\mathrm{LCO}}$ in terms of percent-predicted. The effect size was however low for all these correlations and the corresponding relationships were not observed in any of the other studies. The Befdos study suggested that r_{AiDA} was moderately correlated with the RV and FRC measurements (but not in terms of percent predicted values). The corresponding relationships were not observed in the DW-MRI study.

The SCAPIS data suggested that R_0 was positively correlated with spirometry indices, $\mathrm{D}_{\mathrm{LCO}}$ measurements and X_5 measured with oscillometry and that R_0 was negatively correlated with all other oscillometry variables. However, the effect-size was low for all the correlations. The Befdos-study also suggested that R_0 was positively moderately correlated with VC and with X_5. The other studies, though, did not confirm these relationships or any of the other correlations observed for R_0 in SCAPIS.

AiDA variables explained variance in the SCAPIS data that none of the other lung measurements could explain. Five principal components (PCs) were constructed based on 12 lung measurement indices, including r_{AiDA} and R_0. Figure 11 presents the loadings for each PC. The five PCs explained 39%, 20%, 11%, 9% and 7%, respectively, of the variance in the data. Collectively they explained 86% of the variance in the data. The variance explained by the two PCs with principal loading from the AiDA variables (PC_4 and PC_5) together explained 16% of the total variance in the data.

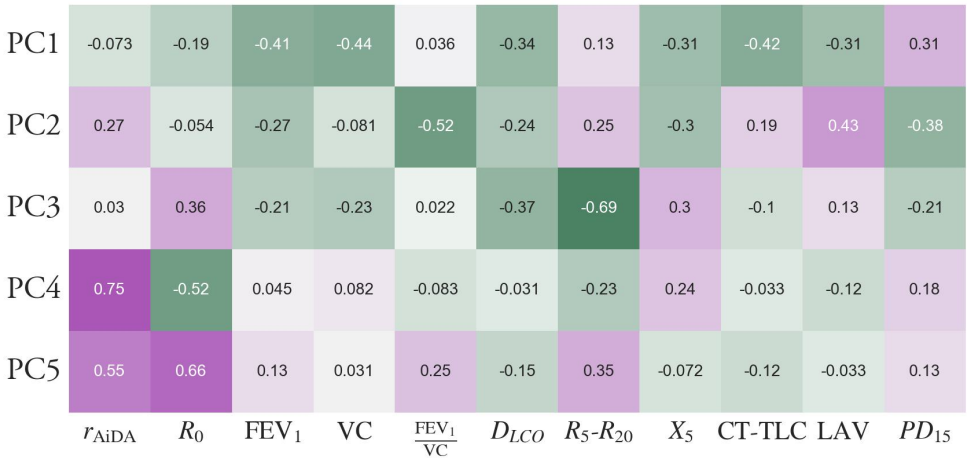

Figure 11: Heatmap of coefficient loadings for principal components PC1-PC5 constructed based on 12 variables in the SCAPIS data set.

4.4 AiDA did not differentiate between welders and controls

AiDA indices were on average not different between welders and controls. Two welders had large airspace radii (374 µm and 385 µm), but these values were not statistically significantly larger than the group average. The average r_{AiDA} for the full study population agreed with measurements of r_{AiDA} measured in the other studies here reported on. Welders and controls had mean r_{AiDA} 290±41 µm and 274 ± 42 µm, respectively. The R_0 was mean 0.51 ±0.23 and 0.55 ±0.20 among welders and controls, respectively. Figure 12A and 12B show the r_{AiDA} and R_0, respectively, for the welders and the controls.

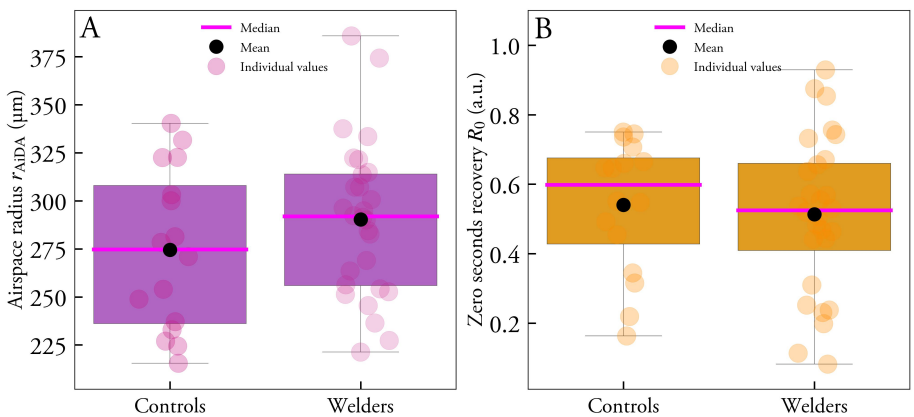

Figure 12: AiDA airspace radius r_{AiDA} (A) and zero seconds recovery R_0 (B) derived from nanoparticle lung deposition measurements in controls and welders.

4.5 AiDA indices and background variables

For all compiled AiDA data, the derived r_{AiDA} values were on average slightly higher among men (291± 40 µm) compared to women (282± 40 µm), but the difference was only just significant (P=0.05). The R_0 values were on average higher for men (0.52± 0.20) compared to women (0.48± 21, (P=0.001)). For the full group the average r_{AiDA} was 287 ±41 µm (with median 282 µm with interquartile range 48 µm) , while the average R_0 was 0.50 ±0.20. Figure 13A shows all calculated r_{AiDA} values, with a log-normal fit with location parameter (log-normal average) 5.6 and scale parameter 0.13. Figure 13B shows all R_0 values, with a normal distribution fit with mean 0.5 and SD 0.2.

The r_{AiDA} was positively correlated with age in all studies (Figure 14). However, the variance in r_{AiDA} was large in all age groups. The r_{AiDA} value ranged between 215 and 320 µm for subjects between 22 and 40 years of age, with mean r_{AiDA} 265 ± 30 µm (N=30). The r_{AiDA} range was 211-444 µm for subjects between 41 and 60 years of age, with mean r_{AiDA} 286 ± 39 µm (N=517). The r_{AiDA} range was 201-580 µm for subjects between 61 and 73 years of age, with mean r_{AiDA} 292 ± 40 µm (N=232). Note however, that the two latter age groups included the subjects that were classified to have emphysema according to CT in the SCAPIS study.

Low effect size associations were observed for r_{AiDA} and R_0 with height and packyears in SCAPIS, but the corresponding associations were not observed in any of the other studies.

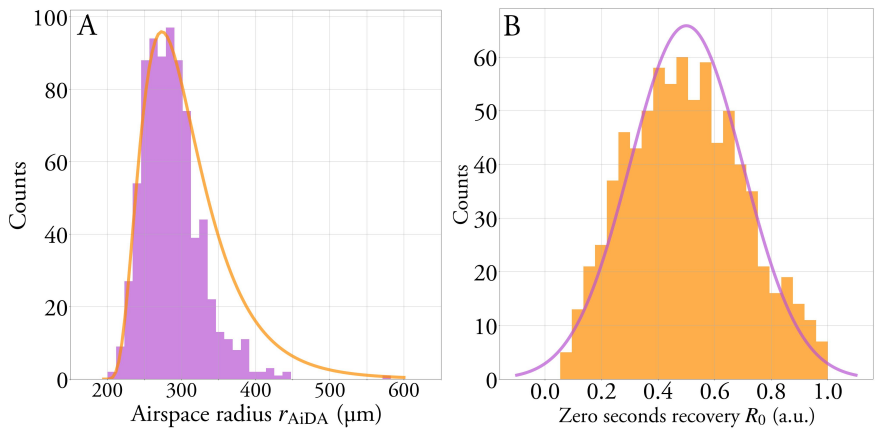

Figure 13: Airspace size r_{AiDA}(A) and zero-seconds recovery R_0(B) distributions for all studies included in this thesis.

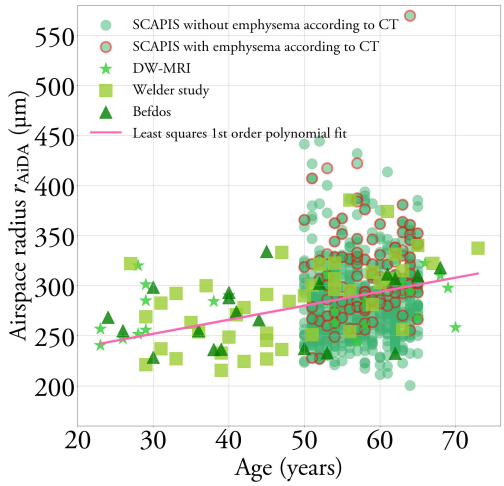

Figure 14: Airspace radius r_{AiDA} as a function of age for all studies presented here. Green circles indicate all participants in the SCAPIS study, where the circles with red borders were the subjects that had emphysema according to CT measurements (visual assessment and LAV>5 %).

4.6 The r_{AiDA} were related to the differences between modeled and measured deposited fraction of 2 µm particles

The modeled DF was significantly correlated with measured DF, for all respiratory tract particle deposition models (P<0.001). However, the measured particle deposition was consistently underestimated by model predictions (Figure 15A). This was the case for all models implemented: ICRP, NCRP, MPPD Y&S, MPPD PNNL and K&H parametrization. The model that best predicted the measured DF was the MPPD model. The difference between modeled and measured DF was significantly linearly correlated with r_{AiDA} measured at half inflation (Figure 15B), for all models. The r_{AiDA} measured at half inflation, with mean 261 $\pm$ 36 µm, was significantly lower than r_{AiDA}, with mean 280$\pm$ 36 µm, measured at full inflation (P<0.001).

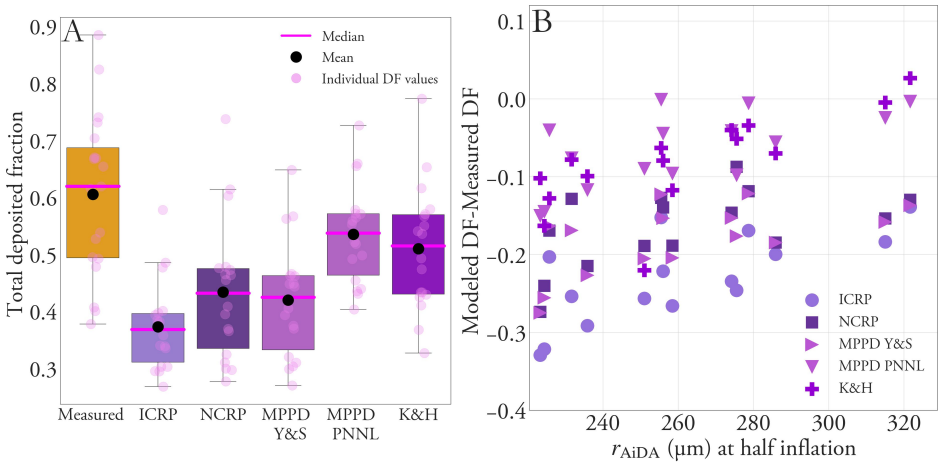

Figure 15: Measured and modeled deposited particle fraction for 2 μm particles (A) and the difference between modeled and measured deposited fraction as a function of r_{AiDA} at half inflation (B).

5 Discussion

The non-invasive approach for distal lung airspace measurements described and evaluated in this thesis is based on the diffusion loss of inhaled nanoparticles as a function of lung residence time. The diffusional losses in the lung deposition measurements are assumed to be primarily related to lung structure, rather than a property of lung function. From the theoretical description, r_{AiDA} is an index related to the size of distal airspaces. The zero seconds recovery, R_0, could be related to particle losses in conducting airways during inhalation and exhalation in the AiDA maneuver, but remains to be further evaluated and interpreted.

5.1 Major findings

AiDA indices correlated with ^{129}Xe DW-MRI diffusion parameters, mean diffusion length scale Lm_D, and α heterogeneity index (Paper I). The r_{AiDA} were larger in participants with emphysema measured with CT (Paper II), which indicated that the AiDA method can potentially be used as a biomarker for emphysema. The AiDA indices, r_{AiDA} and R_0, explained variance in a large data set, which was not explained by other PFT or CT indices (Paper III). This result indicated that the AiDA measurements provided information that was not attainable with the other lung measurements. AiDA indices were poorly, and inconsistently, correlated with standard PFTs and oscillometry measurements (Paper I-V). The r_{AiDA} increased with advancing age, although the r_{AiDA} variance was large for narrow age groups (Papers I-V).

5.2 AiDA in comparison to other lung structure and function measurements

Lung function measurements are accessible in healthcare, while methods for in vivo lung structure assessment are few and expensive. This makes benchmarking of the AiDA method challenging.

Benchmarking AiDA with DW-MRI

With DW-MRI, distal lung microstructures are measured through mapping of the apparent diffusion coefficient ADC: the ADC is elevated due to less restriction in enlarged airspaces. The images generated can provide both regional and local information by measuring ADC. Here, DW-MRI ADC measurements were used to derive full lung mean diffusive length scale Lm_D. In similarity with DW-MRI, AiDA measurements are derived for ventilated areas, i.e. in regions where particles deposit and gas diffuse. In theory, the r_{AiDA} value therefore reflects a quantity similar to Lm_D.

The correlation observed between Lm_D and r_{AiDA}, as well as the correlation between r_{AiDA} and the other diffusion measurements with DW-MRI, suggested that r_{AiDA} is sensitive to distal airspace structure. On a group level, r_{AiDA} and Lm_D agreed. However, as seen in Figure 9A, r_{AiDA} deviated from Lm_D: at smaller airspace sizes Lm_D was in general higher than r_{AiDA}, while the opposite was true for larger airspace sizes. This was also suggested by the Bland-Altman analysis (Figure 9B): r_{AiDA} diverged more from Lm_D with increasing average airspace size.

Several methodological differences can presumably explain some of the deviations observed. While DW-MRI was performed at FRC+1L, a volume approximating VC was inhaled in the AiDA measurements. Previous measurements with ^{3}He DW-MRI have shown that ADC increases with inflation volume (Halaweish et al., 2013). Therefore, AiDA measurements were presumably performed on more inflated distal airspaces compared to the DW-MRI measurements, which could explain why r_{AiDA} values were larger than Lm_D (Figure 9B). Moreover, the r_{AiDA} is interpreted as a rms airspace radius, which means that the value is weighted towards larger airspaces, while Lm_D is not. However, since r_{AiDA} was not consistently larger than Lm_D, these explanations cannot account for the cases when r_{AiDA} was lower than Lm_D.

The two methods measure inherently different phenomena. While DW-MRI measures how much the xenon atoms move (or are restricted to move) the AiDA method measures how many particles that deposit. In contrast with xenon atoms, inhaled nanoparticles deposit when they strike an airspace wall. For DW-MRI, the inhaled xenon atoms have long enough time to encounter distal airspace walls several times over the timescale of milliseconds.

Previous studies have shown that the α heterogeneity index from DW-MRI was decreased due to increasing lung heterogeneity in realistic models of distal airspace geometries derived from CT (Chan et al., 2021) and in COPD patients (Parra-Robles et al., 2013). The comparison between α and the AiDA index R_0 therefore suggests that increased R_0 could be a measure of increasing lung heterogeneity.

The lung images generated with DW-MRI can give regional details on the distribution of lung heterogeneities, while AiDA only provides one geometrical mean airspace radius. This clearly underlines the benefit of DW-MRI. However, since DW-MRI is only available in a few places globally, and requires considerable resources, it cannot be routinely used for diagnosis. In contrast, AiDA measurements are more easily performed and more cost-efficient.

Comparing AiDA with chest CT and pulmonary function tests

Chest CT is the current clinical gold standard for in vivo structural evaluation of emphysema (Gevenois and Yernault, 1995; Gould et al., 1988; Uppaluri et al., 1997) . However, in vivo CT imaging cannot resolve airways smaller than approximately 1.5 mm in diameter (King et al., 1999), corresponding to about the ninth airway generation in the lower respiratory region (see Weibel model, Table 1). Higher resolution is attainable with micro-CT, which has provided 3D visualization of distal airways in ex vivo human lung samples and has been used to investigate COPD mechanisms in small airways and terminal bronchioles (Hogg et al., 2013; McDonough et al., 2011).

The individuals who were identified to have emphysema according to CT in SCAPIS had larger r_{AiDA} compared to non-emphysematous individuals. It should be noted that the SCAPIS study only included one participant who had been diagnosed with emphysema prior to the study, and most participants had normal lung function as measured with standard PFTs. Therefore, the results suggest that r_{AiDA} can be used to identify emphysematous changes in the distal lung. However, not all subjects who had a high r_{AiDA} values had emphysema according to CT. This could either indicate that r_{AiDA} misclassified certain subjects to have increased airspace sizes, or that the associated distal airspace enlargements were not detectable with CT.

The results here presented are also in agreement with previously observed correlations between AiDA and lung density as measured with ^{1}H MRI in a group of 19 never-smoking healthy subjects (Aaltonen et al., 2018b), and higher recovery of nanoparticles in subjects with COPD according to CT, compared to healthy subjects, measured with 19 subjects (Aaltonen et al., 2018a; Jakobsson et al., 2018b). In comparison to CT there is no ionizing radiation dose associated with the AiDA measurements.

With CT, emphysematous regions of the lungs can be identified irrespective of ventilation, while AiDA measurements depend on the distribution of inhaled nanoparticles to the affected regions. In consequence, different types of emphysema could potentially be identified with the two different methods. It can thus be speculated that with AiDA, homogenously distributed emphysema in ventilated regions can be detected, while the method should be less efficient for detection of poorly or less ventilated regions.

Lung function measurements, including spirometry, D_{LCO} and oscillometry, provide average lung function measurements. However, PFTs do not differentiate between emphysema and other causes of airflow obstruction. Therefore, in theory, r_{AiDA} should not necessarily be correlated with lung function measurements, in particular with healthy individuals.

The AiDA method breathing maneuver is closely related to that performed for D_{LCO} measurements, however, the two methods measure two physiologically different characteristics. In similarity with D_{LCO}, the inhalation of particles (gas in the case for D_{LCO}) with the AiDA method starts at RV such that the inhaled aerosol is uniformly spread in the distal lung. The AiDA method is expected to be more influenced by small differences in airspace geometry than the D_{LCO}. Moreover, the D_{LCO} measurements depend on the reaction speed of CO with hemoglobin and a reduced D_{LCO} value is not specific for emphysematous changes (Harvey et al., 2015). While spirometry measurement of FEV_1 and VC is the primary PFT used to detect airflow obstruction, the method has very limited sensitivity to emphysema.

While oscillometry can serve as an alternative to other demanding lung function measurements, AiDA measurements are assumed to be more related to structural changes in the distal lung compared to oscillometry. There were no overall correlations between r_{AiDA} and oscillometry variables, while R_0 was positively correlated with X_5 (Paper III and Paper V), although the effect sizes were low in both cases. Since X_5 has been proposed to be decreased due to ventilation heterogeneity in COPD patients (Crim et al., 2011; Di Mango et al., 2006), this indicated that R_0 is lower due to increasing lung heterogeneity. Note however that the opposite was suggested by the correlation observed between the α heterogeneity index from DW-MRI measurements (Paper I). The relationship between R_0 and X_5 is in line with the previously observed positive correlation between R_0 and FEV_1, evaluated in a small (N=19) group of healthy subjects (Aaltonen et al., 2018a) . Altogether the existing data on R_0 can suggest that R_0 is related to lung function, but more studies are needed to confirm the proposed relationships. If R_0 is decreased due to airflow obstruction, it can theoretically be interpreted as being due to increased particle losses due to turbulent flows in conducting airways caused by the narrowing of airways.

The SCAPIS data gave rise to correlations between AiDA indices and several PFT variables, as well as CT measurements, however in all cases the effect size was low. Since the corresponding correlations were not observed for the smaller studies, it can either be assumed that

the large data in SCAPIS gave rise to arbitrary correlations, or that the sample size in the smaller studies were too low for the corresponding correlations to be observed. However, it should also be noted that in previous studies, with smaller sample sizes (19), it has been observed that the recovery of nanoparticles was correlated with lung function indices, including FEV_1, FEV_1/VC and D_{LCO} (Jakobsson et al., 2018a,b), although not all previous AiDA studies confirmed such relationships (Aaltonen et al., 2018a,b).

5.3 AiDA in comparison to background variables

Women had slightly lower r_{AiDA} than men, although the difference was only just significant. This could be related to the fact that on average, women have smaller lungs than men. However, since r_{AiDA} is in theory only related to distal airspace size, it should not be sex-dependent. Since particle recovery is measured from a volumetric lung depth of 1300 mL for all individuals, the sex-difference observed could indicate that the particle recovery is measured slightly deeper in lungs of women compared to men. However, a previous study of r_{AiDA}, at varying volumetric lung depths, indicated that r_{AiDA} was rather constant at lung depths between 1000 and 2000 mL (J. Jakobsson et al., 2018). On the other hand, that study only included 6 women and 12 men. Here, the measured R_0 was also lower among women compared to men, which can presumably be related to the fact that women have smaller airways than men (Dominelli et al., 2018). If R_0 is related to particle deposition during the dynamic breathing phase in the AiDA maneuver, smaller airways could increase turbulence in the airways, which can enhance particle deposition and ultimately decrease R_0.

The r_{AiDA} was positively correlated with advancing age. This r_{AiDA} age-dependency can be interpreted as an indication of that AiDA measurements are sensitive to age-related airspace size increase (Gillooly & Lamb, 1993). The corresponding increase of Lm_D with advancing age has also been measured with ^{3}He DW-MRI (Fain et al., 2005) (Quirk et al., 2016). However, the r_{AiDA} variance in narrow age groups was also very large, with a range of about 150 µm for subjects between 20 and 50 years of age (r_{AiDA} between 200 and 350 µm), and a range of about 200 µm for individuals aged 50 and above (r_{AiDA} between 200 and 400 µm). It should be underlined that the majority of the AiDA data here studied came from individuals with ages 50-64 years, and more measurements are needed, in particular with subjects at ages below 50 and above 70, to establish how r_{AiDA} depends on age. The wide r_{AiDA} range could also be pointing at individual variations or experimental uncertainties in the measurements that needs to be further taken into account.

The number of packyears were recorded in all studies, except for in the Befdos-study (Paper V). While the SCAPIS study (Paper II and III) suggested that r_{AiDA} was slightly increased with increasing number of packyears, the effect size was low. The other studies (Paper I and Paper IV) did not suggest any relationship between r_{AiDA} and packyears. It can be assumed

that the sample sizes of the studies in Paper I and Paper IV were too small to detect the relationship between r_{AiDA} and packyears, and in particular that the number of subjects with packyears were too low for the relationship to be identified.

5.4 AiDA in an occupational group

Neither r_{AiDA} nor R_0 were on average increased among welders compared to controls (Paper IV). However, two welders had increased airspace sizes, which could indicate that they have pathological changes in the distal lung. None of the other lung function parameters indicated that these two welders had lung function impairments.

Welding fumes putatively cause COPD, but both cross-sectional studies and epidemiological results are inconsistent. Significant declines in lung function indices have been observed to correlate with welding (Chinn et al., 1995, 1990; Wang et al., 1996), but other studies found that lung function only declined when the welders were smokers (Christensen et al., 2008), or when no respiratory protection or ventilation was used (Erkinjuntti-Pekkanen et al., 1999) . The fact that no difference was observed between welders and controls with AiDA can also indicate that the sample size was too low to detect a difference between the groups.

5.5 Can AiDA improve future lung deposition models?

The difference between modeled and measured total deposited fraction of inhaled 2 µm particles during spontaneous breathing, was positively correlated with r_{AiDA} measured at half-inflation. Model calculations of respiratory tract particle deposition are uncertain and fail to accurately capture individual variations. One reason for this are the difficulties associated with modeling the structure and distensibility of the distal lung with geometrically simplified models. If r_{AiDA} can appropriately capture the structure of the distal lung, the AiDA indices could potentially be used for scaling of future distal lung model geometries.

The fact that r_{AiDA} measured at half-inflation, was lower than r_{AiDA} measured at a depth of 1300 mL (Paper V) strengthens the hypothesis that r_{AiDA} is a measure of the average size of the airspaces in the distal lung when assuming a symmetric expansion of the lung.

5.6 Measurement of distal lung structure is tricky

The most popular parameter for assessment of distal lung structure is the mean linear intercept length (Lm). Measurements of Lm are performed using stereological methods (where 2D measurements are translated into 3D geometrical structures) applied to either histology

(lung slices) or to imaging data sets from CT. The Lm metric is considered a mean free distance between distal airspace walls (Knudsen, 2010), however it is often misinterpreted as a mean alveolar size. In principle, stereological methods and standard histology, provide Lm measurements (Hogg et al., 2009; Matsuba and Thurlbeck, 1972). However, the accuracy in estimating distal airspace structure with Lm have caused intensive debates (Weibel et al., 2007; Weibel, 2006; Hsia, 2006; Hsia et al., 2010). This is mainly due to the problems concerning specimen preparation and bias in selection of regions to study in lung parenchyma (Hsia et al., 2010). In view of clinical utility the stereological approaches to assess distal airspace structures are limited by their invasive nature

With Micro-CT, the resolution of standard clinical CT can be increased to visualize the distal airspaces and give estimates of Lm, but such measurements are only available for ex vivo lungs.

The DW-MRI metric Lm_D (D for diffusion) has been interpreted as the same physiological parameter as Lm. The Lm_D metric has been shown to agree with Weibel's model for distal lung structures, as well as with histological measurements (Woods et al., 2006).

Similar to the method proposed in this thesis, aerosol-derived airway morphometry (ADAM), refers to techniques that measure recovery of inhaled particles for measurement of airspace structure (Blanchard, 1996a). With ADAM, particles (typically 0.8-1 µm in diameter) are used to measure particle losses due to settling. From the recovery measurements an effective airspace diameter (EAD) is derived.

The average r_{AiDA} here measured, with overall mean 287 $\pm$41 µm (and range between 200 and 580 µm), corresponds to airway generation 15 and beyond in Weibel's lung model (Table 1). Note however, that r_{AiDA} is derived as a radius and not a diameter. However, since nanoparticles deposit predominantly in distal airspaces, it can be presumed that r_{AiDA} can be considered a geometrical parameter along the line of the Lm definition: a mean free path within the distal airspaces, including alveolar ducts and alveoli, with some possible contribution from higher up airspaces or airways. This definition is also motivated by the correlation observed between r_{AiDA} and Lm_D.

Table 7 outlines some of the available data on Lm from histology and Micro-CT, EAD measured with 1 µm particles, Lm_D derived from DW-MRI, and the r_{AiDA} values presented in this thesis. The outlined results were collected with both healthy patients/lungs, emphysematous patients/lungs, pulmonary fibrosis patients and alpha-1-antitrypsin deficiency (AATD) lungs, for different age groups and varying sample sizes. Since different measurement techniques were used in these studies, important parameters (such as lung inflation) were not necessarily in agreement.

Table 7 shows that the average r_{AiDA} value for this study (for healthy subjects) agreed rather well with the measurements by Kohlhaufl et al. (1999) with ADAM and with Micro-CT

measurements by Tanabe et al. (2017). On average, the derived values for healthy subjects were lower than the average measurements of the controls in those respective studies. The r_{AiDA} values were on average slightly larger than Lm measured with histology and Lm_D measured with DW-MRI.

In relation to the other techniques here discussed AiDA provides one r_{AiDA} value, as opposed to average values derived from pixels in images and the measurements do not require advanced image analysis. While ADAM is no longer in use, DW-MRI is expensive, while Micro-CT and histology are only performed on ex vivo lungs. In clinical practice AiDA could be favorable as a cost efficient and accessible method.

Table 7: Overview of in-vivo and ex-vivo airspace size measurements with different methods: ADAM, histology, Micro-CT, MRI with hyperpolarized gas and AiDA.

Study	Method	Measurement site	N/N_{COPD}	Age range and/or mean± SD	Mean airspace size ± SD (μm)
Kohlhaufl et al. (1999)	ADAM	Distal airspaces	50/20	23-76 56±12	840 ± 530 (COPD) 330 ± 100 (CONTROLS)
Matsuba and Thurlbeck (1972)	Histology	Small airways	12/12	64± 7	744 ± 60
Woods et al. (2006)	Histology	Lm	12/6	-	410 ± 47 (COPD) 200 ± 17 (CONTROLS)
Hogg et al. (2009)	Micro-CT	Lm	8/4	-	150-1200 (COPD) 150 ± 600 (CONTROLS)
Tanabe et al. (2017)	Micro-CT	Lm	20/13	Controls: 56± 7 COPD: 59± 3 AATD: 40±10	336 ± 37 (CONTROLS) 766 ± 259 (COPD) 698 ± 240 COPD-AATD)
Tanabe et al. (2018)	Micro-CT	Lm	15/8	COPD: 56±6 Controls: 59±11	1198 ± 491 (COPD) 390 ± 73 (CONTROLS)
Chan et al. (2019)	^{3}He DW MRI SEM	Lm_D	18/0	71±5.5	272 ± 22 (IPF)
Chan et al. (2018)	^{3}He DW MRI SEM	Lm_D	13/2	45±12	210 ± 7 (CONTROL) 293 ± 30 (COPD)
Chan et al. (2018)	^{129}Xe DW MRI SEM	Lm_D	13/2	45±12	204 ± 8 (CONTROL) 284 ± 33 (COPD)
This study	AiDA		709/70[b]	22-73 COPD: 55±7 Healthy: 58±4	 317±46 (COPD) 281±40 (HEALTHY)

N: number of subjects/specimens, N_{COPD}: number of subjects with COPD or emphysema, SD: standard deviation,Lm: Mean linear intercept,M: number of male subjects, F: number of female subjects,AATD: Alpha-1-Anti-Trypsin deficiency, IPF: idiopathic pulmonary fibrosis.

[b] COPD subjects from SCAPIS, both according to visual assessment and LAV>5% as measured with CT

5.7 Limitations

While r_{AiDA} was larger in subjects with emphysema according to CT-measurements, it is not known how altered ventilation may change the AiDA indices. Lung diseases, such as emphysema and fibrosis, can cause less uniform ventilation in the lungs, and hence less homogenous deposition of nanoparticles. In the studies discussed here, it was assumed that the inhaled nanoparticles reached the acini and deposited uniformly. It was also assumed

that unventilated areas did not contribute to the diffusion losses.

The principal component analysis performed showed that r_{AiDA} and R_0 can be interpreted as new variables for lung measurements and that the variance explained by r_{AiDA} and R_0 are not explained by other lung measurements. However, these results should be interpreted with caution since the PCs primarily determined by r_{AiDA} and R_0 only accounted for 16% of variance in the data. Hence, the AiDA indices do not explain large variations in the data.

The main portion of the participants in the studies were healthy, non-smokers. Most of the AiDA measurement data here analysed were collected in SCAPIS, with a population-based selection of participants in a narrow age range of 50-65 years. Only a small portion (<15%) of the participants in SCAPIS had mild-to-moderate emphysema as measured with CT, and one subject had been diagnosed with COPD. Therefore, the airspace sizes r_{AiDA} measured should in general be viewed to reflect normal healthy distal airspaces. Considering the large sample size contained within SCAPIS, a selection of healthy participants in that study could be used as reference material, for that specific age range, for future AiDA studies.

Airspace radius r_{AiDA} ranged between approximately 200 µm and ∼340 µm for healthy individuals. Lung pathway lengths are not the same to all parts of the respiratory region, which could contribute to variation in the geometrical lung depth at which the main nanoparticle lung deposition occured between individuals. The variation in airspace size can also be attributed to the fact that a considerably lower volume than VC was inhaled in certain AiDA measurements which could results in a higher deposition of nanoparticles in conducting airways. To omit such errors in the future, the AiDA breathing maneuver could be fixed based on lung volume measurements from spirometry to ensure full lung inflation during the experiments.

The recovery values measured were corrected by the experimentally determined C correction factor (Equation 7) as previously described by Jakobsson et al. (2016). If keeping inhaled volume fixed, the correction factor grows exponentially with increasing instrument time $t_{\mathrm{instrument}}$ that the particles spend in the instrument, to correct for the exponential decay of particles. However, the correction also increases with decreasing inhaled volume. The correction dependency on volume should be further investigated, in particular for measurements performed with individuals with smaller lungs, for instance if measuring with AiDA on children.

The spread of r_{AiDA} in narrow age groups points to individual, and possibly experimental and procedural, errors. These include the fact that only an approximate TLC is reached in the AiDA measurements, which could indicate that individual measurements are performed at different lung depths. Moreover, narrowing of conducting airways, could lead to increased particle deposition higher up in the tracheobronchial tree. These matters can bias the recovery measurements, and hence both increase and decrease AiDA indices.

There were large statistical uncertainties associated with determining the average exhaled concentration for very low exhaled concentrations. Since the exhaled concentration is a function of the inhaled concentrations, such uncertainties could be omitted by always requiring a high (> 6000 cm^{-3}) inhaled particle concentration in the AiDA measurements.

It goes without saying that lungs are not strictly structure and function separately. Neither are distal airspaces circular tubes, they are not even spherical. While alveolar ducts more closely resemble tubes, alveoli are described as densely packed polyhedral or inflated ballon-shapes. Moreover, distal airspaces are distensible, and complex entities that are connected with each other.

5.8 Analysis of the recovery data

The analysis procedure for the recovery data was continuously updated throughout this work. The main reason for this, was the eligibility for the analysis to identify points 1-4 in the breathing pattern (see Figure 6A, section 3.2), in an automatic and non-biased way. Since all breathing patterns are different, and the fact that there are no constraints on inhalation and exhalation velocities in the AiDA maneuver, automatic identification of points 1-4 had to be adjusted to various types of breathing patterns.

For this, a set of criteria were checked at the end of the identification of points 1-4 as outlined in section 3.3. These included: the time derivative was equal to zero between points 2 and 4 and the identified duration between points 2-4 was checked to be close to or longer than the instructed breath-hold during the measurements. The time-derivative had to be consistently positive and negative between points 1 and 2 and points 3-4, respectively. If either of these criteria were not fulfilled the breathing pattern was analyzed anew by identification of the plateau in the breathing pattern introduced by the breath-hold time. From identification of this plateau, points 2 and 3 were identified. Further, point 1 was identified as the lowest point within 5 seconds prior to point 2. The remaining points were identified as outlined in section 3.3.

In 95% of all cases, the points in the breathing pattern could be identified with the above outlined procedures. If the points 1-4 were not detected by the automated analysis, I either divided the breathing pattern into sections manually, in order to identify points 1-4 with the above analysis, or discarded the data.

The continuous development of the data-analysis performed for each breathing pattern led to that the SCAPIS data set was different in preparation of paper II compared to in preparation of Paper III. On average, the r_{AiDA} values calculated varied with 10 µm, between the two datasets included in the two separate papers. The individual who had been diagnosed with COPD in the SCAPIS had initially been estimated to have a value of 516 µm, which

at a later stage was identified to be 580 µm.

The resulting breathing pattern during each measurement was dependent on clear instructions from the person performing the measurements with the subject. Most of the measurements here analyzed were performed by medical personnel working at the lung clinic at the Hospital in Malmö. The same personnel also performed the pulmonary function tests.

5.9 Clinical implications

Accurate characterization of emphysema requires diagnostic methods that are non-invasive and sensitive to the regional lung microstructure in the respiratory region of the lungs. The AiDA method might be able to provide this sensitivity. This thesis proposes that the diffusional losses of inhaled nanoparticles, with the AiDA procedure, has potential for identifying changes in the lung structure from emphysema in the distal airspaces in the lungs.

In paper II in this thesis, subjects with mild to moderate CT-measured emphysema showed an increase in the estimated r_{AiDA} when compared to the overall group r_{AiDA}. This increase points to a large potential for clinical applications of AiDA measurements. Since the results demonstrate that r_{AiDA} is sensitive to microstructural features of the distal lung, the method may provide new insights to emphysema progression. However, it is not yet clear what specific features of the lung microstructure that are probed by the inhaled nanoparticle distribution.

AiDA can have the potential to add complementary information about structure to already existing lung function measurements. If R_0 proves to contain lung function information, AiDA would hold both functional and structural information.

AiDA measurements are appealing because they can potentially give simple and direction notion of size of the structural lung units and alterations to it. In principle it would be possible to make the AiDA method portable for it to be used in occupational settings where lung health monitoring can be of importance. The method also has potential in drug development studies. From a clinical perspective its use in characterization of lung structure, where CT and standard lung function tests have limited sensibility, are the likely areas of immediate clinical impact.

6 Future challenges

Further benchmarking of AiDA with DW-MRI measurements is necessary to fully understand how r_{AiDA} is related to Lm_D; the only other in vivo metric of distal airspace structure. Preferably, such studies would be performed with a large variance of distal lung airspace sizes, including variations introduced by emphysema. To fully grasp how lung inflation affects the comparison, AiDA measurements could be performed with varying inhaled volumes to compare with DW-MRI Lm_D.

So far, there is no way of telling if AiDA can separate between restrictive and obstructive lung diseases. In general, for the full understanding of the potential of AiDA, measurements are needed in clinical control studies, with age-matched groups. Subjects with restrictive lung diseases, such as pulmonary fibrosis, and obstructive diseases affecting conducting airways, such as asthma, should be measured with AiDA. These types of measurements are necessary both to understand how r_{AiDA} is affected by different lung conditions, as well as to characterize the R_0 variable.

For future reference there is a need to establish normal, age dependent AiDA values. Based on the measurement performed here, the normal r_{AiDA} for an adult is suggested to range between 200 and $\sim$340 µm, depending on age. To fully capture the age-dependency r_{AiDA} measurements should also be performed with children.

Most of the particle losses in the AiDA setup are due to losses in the flow measurements with the pneumotachograph. In a future setup, these airflow measurements could more easily be performed with less instrument losses by replacing the pneumotachograph with some other flow measurement technique, such as an ultrasound flowmeter.

The AiDA method would be increasingly easy to use and ethically more appreciable if the nanoparticles used in the setup were biodegradable. So far, I am unaware of such hydrophobic particles that could be used for AiDA measurements.

The AiDA setup can be adopted to measure other exhaled quantities in connection with other instruments. In an adjacent study, the AiDA setup was adopted to measure exhaled gases following an exposure in a controlled environment. The subjects were their own controls and the AiDA maneuver was adjusted so that exhaled gases could be quantified with mass spectrometry. The data collected remains to be analyzed and evaluated, however it should be noted that the AiDA setup and maneuver holds great potential for future studies to quantify inhaled and exhaled particles, as well as gases.

7 Conclusions

The short answers to the two questions I set out to address, as outlined in the introduction, are: (1) AiDA measurements were correlated with and of the same order of magnitude of other in vivo (DW-MRI) measurements of distal lung structure measurements and (2) the results here presented indicated that nanoparticle lung deposition measurements contain information beyond that provided by conventional pulmonary function tests.

The results here presented indicated that the AiDA method has potential to characterize distal airspace structure and may serve as a new, non-invasive tool for clinical examination of human lungs. The AiDA method is appealing since it could give direction notion of the distal lung structure, and alterations to it.

It was here shown that airspace radius r_{AiDA} measured with AiDA, correlated with mean diffusion length scale Lm_D from DW-MRI, which is a very advanced and complex measurement technique for distal lung structure assessment. Moreover, r_{AiDA} was increased in subjects with emphysema according to CT assessments, which indicated the potential of AiDA to serve as a clinical biomarker for emphysema.

The measured r_{AiDA} values were poorly correlated with other lung function measurements that are used in clinical practice, which points to the fact that AiDA measurements hold information that are not attainable with standard PFTs. The AiDA zero seconds recovery, R_0, correlated with other measurements related to lung heterogeneity; α heterogeneity index from DW-MRI measurements and oscillometry index X_5. However, R_0 still needs to be further evaluated to make physiological interpretations with the variable.

The r_{AiDA} were positively correlated with age, but not with any other background variables, while R_0 was not found to be related to any background variables.

The AiDA measurements did not differentiate between welders and controls, although two welders had abnormal airspace radii as measured with AiDA. The r_{AiDA} at half-inflation was correlated with the discrepancy observed between modeled and measured micron-sized respiratory tract particle deposition, which suggested that r_{AiDA} at half inflation may serve as an input parameter for future models of respiratory tract particle deposition.

Further validation of the AiDA method in controlled clinical trials are necessary to develop and evaluate the AiDA method as a diagnostic tool. From a practical perspective, there is a need for standardisation of AiDA indices, with respect to age and sex. The AiDA method can be a safe, tolerable and non-ionizing method for investigation of pulmonary structure, and potentially function, with avenues for clinical application in (i) early detection (ii) longitudinal monitoring, (iii) evaluation of treatment response.

8 References

Aaltonen, H., Jakobsson, J., Diaz, S., Zackrisson, S., Piitulainen, E., Löndahl, J., and Wollmer, P. (2018a). Deposition of inhaled nanoparticles is reduced in subjects with copd and correlates with the extent of emphysema: proof of concept for a novel diagnostic technique. *Clinical Physiology and Functional Imaging*, 38(6):1008–1014.

Aaltonen, H. L., Kindvall, S. S., Jakobsson, J. K., Löndahl, J., Olsson, L. E., Diaz, S., Zackrisson, S., and Wollmer, P. (2018b). Airspace dimension assessment with nanoparticles reflects lung density as quantified by mri. *International Journal of Nanomedicine*, 13:2989.

Abramson, M. J., Perret, J. L., Dharmage, S. C., McDonald, V. M., and McDonald, C. F. (2014). Distinguishing adult-onset asthma from copd: a review and a new approach. *International journal of chronic obstructive pulmonary disease*, 9:945.

Adeloye, D., Song, P., Zhu, Y., Campbell, H., Sheikh, A., and Rudan, I. (2022). Global, regional, and national prevalence of, and risk factors for, chronic obstructive pulmonary disease (copd) in 2019: a systematic review and modelling analysis. *The Lancet Respiratory Medicine*, 10(5):447–458.

Anderson, P. J., Wilson, J. D., and Hiller, F. C. (1990). Respiratory tract deposition of ultrafine particles in subjects with obstructive or restrictive lung disease. *Chest*, 97(5):1115–1120.

Asgharian, B., Hofmann, W., and Bergmann, R. (2001). Particle deposition in a multiple-path model of the human lung. *Aerosol Science & Technology*, 34(4):332–339.

Bennett, W. D. and Smaldone, G. C. (1988). Use of aerosols to estimate mean air-space size in chronic obstructive pulmonary disease. *Journal of Applied Physiology*, 64(4):1554–1560.

Berberan-Santos, M., Bodunov, E., and Valeur, B. (2005). Mathematical functions for the analysis of luminescence decays with underlying distributions 1. kohlrausch decay function (stretched exponential). *Chemical Physics*, 315(1-2):171–182.

Blanchard, J. D. (1996a). Aerosol bolus dispersion and aerosol-derived airway morphometry: assessment of lung pathology and response to therapy, part 1. *Journal of aerosol medicine*, 9(2):183–205.

Blanchard, J. D. (1996b). Aerosol bolus dispersion and aerosol-derived airway morphometry: assessment of lung pathology and response to therapy, part 2. *Journal of aerosol medicine*, 9(4):453–476.

Brand, P., Rieger, C., Beinert, T., and Heyder, J. (1995). Aerosol derived airway morphometry in healthy subjects. *European Respiratory Journal*, 8(10):1639–1646.

Brown, J. S., Zeman, K. L., and Bennett, W. D. (2002). Ultrafine particle deposition and clearance in the healthy and obstructed lung. *American journal of respiratory and critical care medicine*, 166(9):1240–1247.

Burgel, P., De Blic, J., Chanez, P., Delacourt, C., Devillier, P., Didier, A., Dubus, J., Frachon, I., Garcia, G., Humbert, M., et al. (2009). Update on the roles of distal airways in asthma. *European Respiratory Review*, 18(112):80–95.

Burney, P. G., Patel, J., Newson, R., Minelli, C., and Naghavi, M. (2015). Global and regional trends in copd mortality, 1990–2010. *European Respiratory Journal*, 45(5):1239–1247.

Chalupa, D. C., Morrow, P. E., Oberdörster, G., Utell, M. J., and Frampton, M. W. (2004). Ultrafine particle deposition in subjects with asthma. *Environmental health perspectives*, 112(8):879–882.

Chan, H.-F., Collier, G. J., Parra-Robles, J., and Wild, J. M. (2021). Finite element simulations of hyperpolarized gas dwi in micro-ct meshes of acinar airways: validating the cylinder and stretched exponential models of lung microstructural length scales. *Magnetic Resonance in Medicine*, 86(1):514–525.

Chan, H.-F., Stewart, N. J., Norquay, G., Collier, G. J., and Wild, J. M. (2018). 3d diffusion-weighted 129xe mri for whole lung morphometry. *Magnetic Resonance in Medicine*, 79(6):2986–2995.

Chan, H.-F., Weatherley, N. D., Johns, C. S., Stewart, N. J., Collier, G. J., Bianchi, S. M., and Wild, J. M. (2019). Airway microstructure in idiopathic pulmonary fibrosis: assessment at hyperpolarized 3he diffusion-weighted mri. *Radiology*, 291(1):223–229.

Chinn, D., Cotes, J., El Gamal, F., and Wollaston, J. (1995). Respiratory health of young shipyard welders and other tradesmen studied cross sectionally and longitudinally. *Occupational and environmental medicine*, 52(1):33–42.

Chinn, D., Stevenson, I., and Cotes, J. (1990). Longitudinal respiratory survey of shipyard workers: effects of trade and atopic status. *Occupational and Environmental Medicine*, 47(2):83–90.

Christensen, S. W., Bonde, J. P., and Omland, Ø. (2008). A prospective study of decline in lung function in relation to welding emissions. *Journal of Occupational Medicine and Toxicology*, 3(1):1–8.

Criée, C., Sorichter, S., Smith, H., Kardos, P., Merget, R., Heise, D., Berdel, D., Köhler, D., Magnussen, H., Marek, W., et al. (2011). Body plethysmography–its principles and clinical use. *Respiratory medicine*, 105(7):959–971.

Crim, C., Celli, B., Edwards, L. D., Wouters, E., Coxson, H. O., Tal-Singer, R., Calverley, P. M., investigators, E., et al. (2011). Respiratory system impedance with impulse oscillometry in healthy and copd subjects: Eclipse baseline results. *Respiratory medicine*, 105(7):1069–1078.

Di Mango, A. M. G., Lopes, A. J., Jansen, J. M., and Melo, P. L. (2006). Changes in respiratory mechanics with increasing degrees of airway obstruction in copd: detection by forced oscillation technique. *Respiratory medicine*, 100(3):399–410.

Dominelli, P. B., Ripoll, J. G., Cross, T. J., Baker, S. E., Wiggins, C. C., Welch, B. T., and Joyner, M. J. (2018). Sex differences in large conducting airway anatomy. *Journal of Applied Physiology*, 125(3):960–965.

Doorly, D., Taylor, D., Gambaruto, A., Schroter, R., and Tolley, N. (2008). Nasal architecture: form and flow. *Philosophical Transactions of the Royal Society A: Mathematical, Physical and Engineering Sciences*, 366(1879):3225–3246.

Erkinjuntti-Pekkanen, R., Slater, T., Cheng, S., Fishwick, D., Bradshaw, L., Kimbell-Dunn, M., Dronfield, L., and Pearce, N. (1999). Two year follow up of pulmonary function values among welders in new zealand. *Occupational and Environmental Medicine*, 56(5):328–333.

Fain, S. B., Altes, T. A., Panth, S. R., Evans, M. D., Waters, B., Mugler III, J. P., Korosec, F. R., Grist, T. M., Silverman, M., Salerno, M., et al. (2005). Detection of age-dependent changes in healthy adult lungs with diffusion-weighted 3he mri. *Academic radiology*, 12(11):1385–1393.

Faria, A. C., Lopes, A. J., Jansen, J. M., and Melo, P. L. (2009). Evaluating the forced oscillation technique in the detection of early smoking-induced respiratory changes. *Biomedical engineering online*, 8(1):1–10.

Faria, A. C. D., da Costa, A. A., Lopes, A. J., Jansen, J. M., and de Melo, P. L. (2010). Forced oscillation technique in the detection of smoking-induced respiratory alterations: diagnostic accuracy and comparison with spirometry. *Clinics*, 65(12):1295–1304.

Gebhart, J., Heyder, J., and Stahlhofen, W. (1981). Use of aerosols to estimate pulmonary air-space dimensions. *Journal of Applied Physiology*, 51(2):465–476.

Gevenois, P.-A. and Yernault, J. C. (1995). Can computed tomography quantify pulmonary emphysema? *European Respiratory Journal*, 8(5):843–848.

Gillooly, M. and Lamb, D. (1993). Airspace size in lungs of lifelong non-smokers: effect of age and sex. *Thorax*, 48(1):39–43.

Goldberg, I. S. and Smith, R. B. (1981). Settling and diffusion of aerosol particles in small airways during breath holding. *Annals of Biomedical Engineering*, 9(5):557–575.

Gould, G., MacNee, W., McLean, A., Warren, P., Redpath, A., Best, J., Lamb, D., and Flenley, D. (1988). Ct measurements of lung density in life can quantitate distal airspace enlargement—an essential defining feature of human emphysema. *American Review of Respiratory Disease*, 137(2):380–392.

Gurney, J. W., Jones, K. K., Robbins, R. A., Gossman, G. L., Nelson, K. J., Daughton, D., Spurzem, J. R., and Rennard, S. I. (1992). Regional distribution of emphysema: correlation of high-resolution ct with pulmonary function tests in unselected smokers. *Radiology*, 183(2):457–463.

Hajari, A. J., Yablonskiy, D. A., Sukstanskii, A. L., Quirk, J. D., Conradi, M. S., and Woods, J. C. (2012). Morphometric changes in the human pulmonary acinus during inflation. *Journal of applied physiology*, 112(6):937–943.

Halaweish, A. F., Hoffman, E. A., Thedens, D. R., Fuld, M. K., Sieren, J. P., and van Beek, E. J. (2013). Effect of lung inflation level on hyperpolarized 3he apparent diffusion coefficient measurements in never-smokers. *Radiology*, 268(2):572.

Harvey, B.-G., Strulovici-Barel, Y., Kaner, R. J., Sanders, A., Vincent, T. L., Mezey, J. G., and Crystal, R. G. (2015). Risk of copd with obstruction in active smokers with normal spirometry and reduced diffusion capacity. *European Respiratory Journal*, 46(6):1589–1597.

Higham, A., Quinn, A. M., Cançado, J. E. D., and Singh, D. (2019). The pathology of small airways disease in copd: historical aspects and future directions. *Respiratory research*, 20(1):1–11.

Hinds, C. (1999). Aerosol technology, 2nd edn new york. *NY John Wiley & Sons*.

Hofemeier, P. and Sznitman, J. (2015). Revisiting pulmonary acinar particle transport: convection, sedimentation, diffusion, and their interplay. *Journal of Applied Physiology*, 118(11):1375–1385.

Hofmann, W. (2011). Modelling inhaled particle deposition in the human lung—a review. *Journal of Aerosol Science*, 42(10):693–724.

Hogg, J. C., McDonough, J. E., Sanchez, P. G., Cooper, J. D., Coxson, H. O., Elliott, W. M., Naiman, D., Pochettino, M., Horng, D., Gefter, W. B., et al. (2009). Micro–computed tomography measurements of peripheral lung pathology in chronic obstructive pulmonary disease. *Proceedings of the American Thoracic Society*, 6(6):546–549.

Hogg, J. C., McDonough, J. E., and Suzuki, M. (2013). Small airway obstruction in copd: new insights based on micro-ct imaging and mri imaging. *Chest*, 143(5):1436–1443.

Hsia, C. (2006). Quantitative morphology of compensatory lung growth. *European Respiratory Review*, 15(101):148–156.

Hsia, C. C., Hyde, D. M., Ochs, M., and Weibel, E. R. (2010). An official research policy statement of the american thoracic society/european respiratory society: standards for quantitative assessment of lung structure. *American journal of respiratory and critical care medicine*, 181(4):394–418.

Hussein, T., Saleh, S. S. A., dos Santos, V. N., Boor, B. E., Koivisto, A. J., and Löndahl, J. (2019). Regional inhaled deposited dose of urban aerosols in an eastern mediterranean city. *Atmosphere*, 10(9):530.

Iwano, S., Okada, T., Satake, H., and Naganawa, S. (2009). 3d-ct volumetry of the lung using multidetector row ct: comparison with pulmonary function tests. *Academic radiology*, 16(3):250–256.

Jakobsson, J., Wollmer, P., and Löndahl, J. (2018a). Charting the human respiratory tract with airborne nanoparticles: evaluation of the airspace dimension assessment technique. *Journal of Applied Physiology*, 125(6):1832–1840.

Jakobsson, J. K., Aaltonen, H. L., Nicklasson, H., Gudmundsson, A., Rissler, J., Wollmer, P., and Löndahl, J. (2018b). Altered deposition of inhaled nanoparticles in subjects with chronic obstructive pulmonary disease. *BMC pulmonary medicine*, 18(1):1–11.

Jakobsson, J. K., Hedlund, J., Kumlin, J., Wollmer, P., and Löndahl, J. (2016). A new method for measuring lung deposition efficiency of airborne nanoparticles in a single breath. *Scientific Reports*, 6(1):1–10.

Jetmalani, K., Thamrin, C., Farah, C. S., Bertolin, A., Chapman, D. G., Berend, N., Salome, C. M., and King, G. G. (2018). Peripheral airway dysfunction and relationship with symptoms in smokers with preserved spirometry. *Respirology*, 23(5):512–518.

Kaminsky, D. A., Simpson, S. J., Berger, K. I., Calverley, P., de Melo, P. L., Dandurand, R., Dellacà, R. L., Farah, C. S., Farré, R., Hall, G. L., et al. (2022). Clinical significance and applications of oscillometry. *European Respiratory Review*, 31(163).

Kaur, S., Nieuwenhuijsen, M., and Colvile, R. (2005). Pedestrian exposure to air pollution along a major road in central london, uk. *Atmospheric Environment*, 39(38):7307–7320.

Kaushik, S. S., Cleveland, Z. I., Cofer, G. P., Metz, G., Beaver, D., Nouls, J., Kraft, M., Auffermann, W., Wolber, J., McAdams, H. P., et al. (2011). Diffusion-weighted hyperpolarized 129xe mri in healthy volunteers and subjects with chronic obstructive pulmonary disease. *Magnetic Resonance in Medicine*, 65(4):1154–1165.

Ketzel, M., Wåhlin, P., Berkowicz, R., and Palmgren, F. (2003). Particle and trace gas emission factors under urban driving conditions in copenhagen based on street and roof-level observations. *Atmospheric Environment*, 37(20):2735–2749.

Kim, C. S. and Hu, S.-C. (2006). Total respiratory tract deposition of fine micrometer-sized particles in healthy adults: empirical equations for sex and breathing pattern. *Journal of Applied Physiology*, 101(2):401–412. PMID: 16849812.

King, G. G., Muller, N. L., and Pare, P. D. (1999). Evaluation of airways in obstructive pulmonary disease using high-resolution computed tomography. *American journal of respiratory and critical care medicine*, 159(3):992–1004.

Kirby, M., Ouriadov, A., Svenningsen, S., Owrangi, A., Wheatley, A., Etemad-Rezai, R., Santyr, G. E., McCormack, D. G., and Parraga, G. (2014). Hyperpolarized 3he and 129xe magnetic resonance imaging apparent diffusion coefficients: physiological relevance in older never-and ex-smokers. *Physiological reports*, 2(7):e12068.

Kirby, M., Svenningsen, S., Owrangi, A., Wheatley, A., Farag, A., Ouriadov, A., Santyr, G. E., Etemad-Rezai, R., Coxson, H. O., McCormack, D. G., et al. (2012). Hyperpolarized 3he and 129xe mr imaging in healthy volunteers and patients with chronic obstructive pulmonary disease. *Radiology*, 265(2):600.

Koblinger, L. and Hofmann, W. (1990). Monte carlo modeling of aerosol deposition in human lungs. part i: Simulation of particle transport in a stochastic lung structure. *Journal of Aerosol Science*, 21(5):661–674.

Kohlhaufl, M., Brand, P., Rock, C., Radons, T., Scheuch, G., Meyer, T., Schulz, H., Pfeifer, K. J., Haussinger, K., and Heyder, J. (1999). Noninvasive diagnosis of emphysema: aerosol morphometry and aerosol bolus dispersion in comparison to hrct. *American journal of respiratory and critical care medicine*, 160(3):913–918.

Lapp, N., Hankinson, J., Amandus, H., and Palmes, E. (1975). Variability in the size of airspaces in normal human lungs as estimated by aerosols. *Thorax*, 30(3):293–299.

Löndahl, J., Jakobsson, J. K., Broday, D. M., Aaltonen, H. L., and Wollmer, P. (2017). Do nanoparticles provide a new opportunity for diagnosis of distal airspace disease? *International Journal of nanomedicine*, 12:41.

Löndahl, J., Möller, W., Pagels, J. H., Kreyling, W. G., Swietlicki, E., and Schmid, O. (2014). Measurement techniques for respiratory tract deposition of airborne nanoparticles: a critical review. *Journal of aerosol medicine and pulmonary drug delivery*, 27(4):229–254.

Löndahl, J., Swietlicki, E., Rissler, J., Bengtsson, A., Boman, C., Blomberg, A., and Sandström, T. (2012). Experimental determination of the respiratory tract deposition of diesel combustion particles in patients with chronic obstructive pulmonary disease. *Particle and Fibre Toxicology*, 9(1):1–8.

Longley, I., Gallagher, M., Dorsey, J., and Flynn, M. (2004). A case-study of fine particle concentrations and fluxes measured in a busy street canyon in manchester, uk. *Atmospheric Environment*, 38(22):3595–3603.

Marrades, R. M., Diaz, O., Roca, J., Campistol, J. M., Torregrosa, J. V., Barberà, J. A., Cobos, A., Felez, M. A., and Rodriguez-Roisin, R. (1997). Adjustment of dlco for hemoglobin concentration. *American journal of respiratory and critical care medicine*, 155(1):236–241.

Matsuba, K. and Thurlbeck, W. M. (1972). The number and dimensions of small airways in emphysematous lungs. *The American Journal of Pathology*, 67(2):265.

McDonough, J. E., Yuan, R., Suzuki, M., Seyednejad, N., Elliott, W. M., Sanchez, P. G., Wright, A. C., Gefter, W. B., Litzky, L., Coxson, H. O., et al. (2011). Small-airway obstruction and emphysema in chronic obstructive pulmonary disease. *New England Journal of Medicine*, 365(17):1567–1575.

Moller, W., Felten, K., Sommerer, K., Scheuch, G., Meyer, G., Meyer, P., Haussinger, K., and Kreyling, W. G. (2008). Deposition, retention, and translocation of ultrafine particles from the central airways and lung periphery. *American journal of respiratory and critical care medicine*, 177(4):426–432.

NCRP (1997). Deposition, retention, and dosimetry of inhaled radioactivesubstances, ncrp report. 125.

Ochs, M., Nyengaard, J. R., Jung, A., Knudsen, L., Voigt, M., Wahlers, T., Richter, J., and Gundersen, H. J. G. (2004). The number of alveoli in the human lung. *American journal of respiratory and critical care medicine*, 169(1):120–124.

Olsson, B. and Bäckman, P. (2018). Mimetikos preludium™: a new pharma-friendly aerosol drug deposition calculator. In *Respiratory Drug Delivery*, volume 1, pages 103–112. Davis Healthcare International Publishing, LLC.

Olvera, H. A., Perez, D., Clague, J. W., Cheng, Y.-S., Li, W.-W., Amaya, M. A., Burchiel, S. W., Berwick, M., and Pingitore, N. E. (2012). The effect of ventilation, age, and asthmatic condition on ultrafine particle deposition in children. *Pulmonary medicine*, 2012.

Palmes, E. (1968). Use of aerosols to measure pulmonary dimensions. *Journal of the Air Pollution Control Association*, 18(10):671–671.

Palmes, E. D. (1973). Measurement of pulmonary air spaces using aerosols. *Archives of Internal Medicine*, 131(1):76–79.

Papadakos, P. J. and Lachmann, B. (2007). Mechanical ventilation e-book: Clinical applications and pathophysiology.

Quirk, J. D., Sukstanskii, A. L., Woods, J. C., Lutey, B. A., Conradi, M. S., Gierada, D. S., Yusen, R. D., Castro, M., and Yablonskiy, D. A. (2016). Experimental evidence of age-related adaptive changes in human acinar airways. *Journal of Applied Physiology*, 120(2):159–165.

Saam, B. T., Yablonskiy, D. A., Kodibagkar, V. D., Leawoods, J. C., Gierada, D. S., Cooper, J. D., Lefrak, S. S., and Conradi, M. S. (2000). Mr imaging of diffusion of 3he gas in healthy and diseased lungs. *Magnetic Resonance in Medicine: An Official Journal of the International Society for Magnetic Resonance in Medicine*, 44(2):174–179.

Schittny, J. C. (2017). Development of the lung. *Cell and tissue research*, 367(3):427–444.

Shinke, H., Yamamoto, M., Hazeki, N., Kotani, Y., Kobayashi, K., and Nishimura, Y. (2013). Visualized changes in respiratory resistance and reactance along a time axis in smokers: a cross-sectional study. *Respiratory investigation*, 51(3):166–174.

Smith, H. (1994). Human respiratory tract model for radiological protection. *ICRP publication 66*.

Stolk, J. and Stoel, B. C. (2011). Lung densitometry to assess progression of emphysema in chronic obstructive pulmonary disease: time to apply in the clinic?

Tanabe, N., Vasilescu, D. M., Kirby, M., Coxson, H. O., Verleden, S. E., Vanaudenaerde, B. M., Kinose, D., Nakano, Y., Paré, P. D., and Hogg, J. C. (2018). Analysis of airway pathology in copd using a combination of computed tomography, micro-computed tomography and histology. *European Respiratory Journal*, 51(2).

Tanabe, N., Vasilescu, D. M., McDonough, J. E., Kinose, D., Suzuki, M., Cooper, J. D., Paré, P. D., and Hogg, J. C. (2017). Micro–computed tomography comparison of preterminal bronchioles in centrilobular and panlobular emphysema. *American journal of respiratory and critical care medicine*, 195(5):630–638.

Thurlbeck, W. (1995). Chronic airflow obstruction. in. *Pathology of the lung*, 780.

Torén, K., Olin, A.-C., Lindberg, A., Vikgren, J., Schiöler, L., Brandberg, J., Johnsson, Å., Engström, G., Persson, H. L., Sköld, M., et al. (2016). Vital capacity and copd: the swedish cardiopulmonary bioimage study (scapis). *International journal of chronic obstructive pulmonary disease*, 11:927.

Tsuda, A., Henry, F. S., and Butler, J. P. (1995). Chaotic mixing of alveolated duct flow in rhythmically expanding pulmonary acinus. *Journal of Applied Physiology*, 79(3):1055–1063.

Uppaluri, R., Mitsa, T., Sonka, M., Hoffman, E. A., and McLennan, G. (1997). Quantification of pulmonary emphysema from lung computed tomography images. *American journal of respiratory and critical care medicine*, 156(1):248–254.

Vogelmeier, C. F., Criner, G. J., Martinez, F. J., Anzueto, A., Barnes, P. J., Bourbeau, J., Celli, B. R., Chen, R., Decramer, M., Fabbri, L. M., et al. (2017). Global strategy for the diagnosis, management, and prevention of chronic obstructive lung disease 2017 report. gold executive summary. *American journal of respiratory and critical care medicine*, 195(5):557–582.

Wang, C.-s. (2005). *Inhaled particles*. Elsevier.

Wang, M.-L., McCabe, L., Hankinson, J. L., Shamssain, M. H., Gunel, E., Lapp, N., and Banks, D. E. (1996). Longitudinal and cross-sectional analyses of lung function in steelworkers. *American journal of respiratory and critical care medicine*, 153(6):1907–1913.

Weibel, E. R. (1991). Fractal geometry: a design principle for living organisms. *American Journal of Physiology-Lung Cellular and Molecular Physiology*, 261(6):L361–L369.

Weibel, E. R. (2006). Morphological quantitation of emphysema: a debate. *Journal of Applied Physiology*, 100(4):1419–1421.

Weibel, E. R. (2017). Lung morphometry: the link between structure and function. *Cell and tissue research*, 367(3):413–426.

Weibel, E. R., Cournand, A. F., and Richards, D. W. (1963). *Morphometry of the human lung*, volume 1. Springer.

Weibel, E. R., Hsia, C. C., and Ochs, M. (2007). How much is there really? why stereology is essential in lung morphometry. *Journal of applied physiology*, 102(1):459–467.

Woods, J. C., Choong, C. K., Yablonskiy, D. A., Bentley, J., Wong, J., Pierce, J. A., Cooper, J. D., Macklem, P. T., Conradi, M. S., and Hogg, J. C. (2006). Hyperpolarized 3he diffusion mri and histology in pulmonary emphysema. *Magnetic Resonance in Medicine: An Official Journal of the International Society for Magnetic Resonance in Medicine*, 56(6):1293–1300.

Yablonskiy, D. A., Sukstanskii, A. L., Woods, J. C., Gierada, D. S., Quirk, J. D., Hogg, J. C., Cooper, J. D., and Conradi, M. S. (2009). Quantification of lung microstructure with hyperpolarized 3he diffusion mri. *Journal of applied physiology*, 107(4):1258–1265.

Yeh, H.-C. and Schum, G. (1980). Models of human lung airways and their application to inhaled particle deposition. *Bulletin of mathematical biology*, 42(3):461–480.

Yu, C., Liu, C., and Taulbee, D. (1977). Simultaneous diffusion and sedimentation of aerosols in a horizontal cylinder. *Journal of Aerosol Science*, 8(5):309–316.

Scientific publications

Printed by Media-Tryck, Lund 2023 NORDIC SWAN ECOLABEL 3041 0903

Faculty of Engineering
Department of Design Sciences

ISBN 978-91-8039-539-7